Modeling the Synergy of Cofilin and Arp2/3 in Lamellipodial Protrusive Activity

Nessy Tania,[†‡] John Condeelis,[§] and Leah Edelstein-Keshet[†*]
[†]Department of Mathematics, University of British Columbia, Vancouver, Canada; [‡]Department of Mathematics and Statistics, Smith College, Northampton, Massachusetts; and [§]Department of Anatomy and Structural Biology, Gruss Lipper Biophotonics Center, Albert Einstein College of Medicine of Yeshiva University, Bronx, New York

ABSTRACT Rapid polymerization of actin filament barbed ends generates protrusive forces at the cell edge, leading to cell migration. Two important regulators of free barbed ends, cofilin and Arp2/3, have been shown to work in synergy (net effect greater than additive). To explore this synergy, we model the dynamics of F-actin at the leading edge, motivated by data from EGF-stimulated mammary carcinoma cells. We study how synergy depends on the localized rates and relative timing of cofilin and Arp2/3 activation at the cell edge. The model incorporates diffusion of cofilin, membrane protrusion, F-actin capping, aging, and severing by cofilin and branch nucleation by Arp2/3 (but not G-actin recycling). In a well-mixed system, cofilin and Arp2/3 can each generate a large pulse of barbed ends on their own, but have little synergy; high synergy occurs only at low activation rates, when few barbed ends are produced. In the full spatially distributed model, both synergy and barbed-end production are significant over a range of activation rates. Furthermore, barbed-end production is greatest when Arp2/3 activation is delayed relative to cofilin. Our model supports a direct role for cofilin-mediated actin polymerization in stimulated cell migration, including chemotaxis and cancer invasion.

INTRODUCTION

In motile eukaryotic cells, actin filaments grow, push on the cell edge, and empower cell motility. New growing (barbed) ends of F-actin are formed by Arp2/3-mediated branching (1–4) and by cofilin severing of F-actin mother filaments. Barbed-end production by cofilin is observed experimentally (1,5–7), and complements cofilin's other well-established role of recycling F-actin into monomers (8–10). Arp2/3 and cofilin have been shown to work in synergy to generate new actin barbed ends (11), motivating our model.

The control of actin filament dynamics by regulatory proteins such as cofilin and Arp2/3 is known to depend on the nucleotide-state (or age) of the actin. Arp2/3 forms a more stable branch on the side of ATP or ADP-Pi filament with a 10-fold increase in dissociation as the mother filament ages (12). Cofilin binds and severs almost 40× preferentially to ADP-F-actin (13). The barbed ends created by cofilin polymerize new ATP-F-actin, forming preferential binding sites for Arp2/3 complexes (12,14). Cofilin also accelerates the release of the phosphate (Pi) group and promotes debranching of filaments (14), as well as recycling actin filaments and replenishing the G-actin pool, roles we do not discuss here. The conversion from ATP to ADP F-actin state in vivo has been shown to occur within 10–30 s (3,13,15) (whereas, in vitro, Pi release occurs more slowly, at a timescale of minutes (16–18)).

Motivation for our model in this article stems from the experimentally observed actin-based protrusion after epidermal growth factor (EGF) stimulation in mammary carcinoma cells. In these cells, both cofilin and Arp2/3 are activated at the membrane. Active cofilin diffuses into the lamellipod (6), while active Arp2/3 is anchored to the WAVE2 complex (WASP-family verprolin homologous protein) at the leading edge (19–21). After EGF stimulation, cofilin is rapidly activated and released from the cell membrane. Here we focus on modeling early spatio-temporal actin dynamics after stimulation to characterize where, when, and how cofilin function could generate new barbed ends. The critical role of cofilin in regulating the spatiotemporal dynamics of actin cytoskeleton has been observed in a diverse array of processes from morphogenesis, receptor trafficking in synapses, and inflammation (22,23), further motivating our model.

In mammary carcinoma cells, a large peak of cofilin-dependent barbed ends is observed at 1 min after EGF stimulation (1,5,7). Given the ample availability of G-actin in the cytosol, growth of these barbed ends rapidly produces new F-actin, promoting Arp2/3 nucleation of a second peak of barbed ends ~2 min later (24). To understand this synergy between cofilin and Arp2/3 (11), we use a mathematical model for actin dynamics at the leading edge of a motile cell. Specifically, we aim to address the following questions:

1. How does cofilin-Arp2/3 synergy depend on biochemical parameters?
2. How does the relative timing of Arp2/3 and cofilin stimulation affect synergy?
3. How does spatial localization affect synergy and barbed-end production?

Submitted February 6, 2013, and accepted for publication September 16, 2013.

*Correspondence: keshet@math.ubc.ca

Editor: Cecile Sykes.

0006-3495/13/11/1946/10 $2.00

http://dx.doi.org/10.1016/j.bpj.2013.09.013

MATHEMATICAL MODEL

We consider a narrow transect of the lamellipod, a thin flat region ~10 μm at the leading edge of the cell. We keep track of the length density of F-actin filaments and the corresponding barbed-end density, as well as the concentrations of active cofilin and Arp2/3 (see Fig. 1 for the geometry and schematic diagram). We discuss the model components first in a well-mixed null model and then in the fully spatiotemporal version.

Well-mixed model

The assumptions and corresponding (well-mixed) model equations are as follows:

Assumption 1

ATP F-actin (length density $F_{\rm new}$) polymerizes from free barbed ends (number density B) at speed V_0 (assumed constant) and ages into ADP F-actin, $F_{\rm old}$, at rate $k_{\rm age}$. J_f is a small basal actin polymerization from other sources (e.g., formin (21,25)). Hence,

$$\frac{dF_{\rm new}}{dt} = J_f - k_{\rm age}\,F_{\rm new} + V_0\,B. \tag{1}$$

Assumption 2

We assume bulk turnover of old F-actin (rate $k_{\rm deg}$), as in, for example (8,26,27)

$$\frac{dF_{\rm old}}{dt} = k_{\rm age}\,F_{\rm new} - k_{\rm deg}\,F_{\rm old}. \tag{2}$$

This typical assumption replaces an older view of depolymerization at pointed ends.

Assumption 3

Cofilin, C, is transiently activated (step function $J_C(t)$), and depleted by inactivation (rate k_c), and by binding and severing old ADP-F-actin (rate $f_{\rm sev}$ as in Tania et al. (28)). Hence,

$$\begin{aligned}\frac{dC}{dt} &= J_C(t) - k_cC - f_{\rm sev},\\ \text{where } f_{\rm sev}(C,F_{\rm old}) &= k_{\rm sev}C_0\left(\frac{C}{C_0}\right)^n \ell F_{\rm old}.\end{aligned} \tag{3}$$

We have shown that this nonlinear severing rate, possibly reflecting cooperativity (29), is needed for the large stimulus-induced amplification of barbed ends (28). Here, C_0 is a typical cofilin concentration at which significant severing activity is observed and ℓ converts F-actin length density to a concentration. After severing, cofilin must be phosphorylated and then reactivated at the membrane on a slower timescale, a process not modeled here (but see Tania et al. (28)).

Assumption 4

Similarly, Arp2/3, A, is activated (step function $J_A(t)$), and depleted by inactivation (rate k_a), and by binding to ATP-F-actin, $F_{\rm new}$. This rate of branching, which nucleates barbed ends, is assumed proportional to $F_{\rm new}$ and saturating in A (26). Thus,

$$\begin{aligned}\frac{dA}{dt} &= J_A(t) - k_aA - f_{\rm nuc},\\ \text{where } f_{\rm nuc}(A,F_{\rm new}) &= k_{\rm nuc}\frac{A}{K_m + A}\,\ell F_{\rm new}.\end{aligned} \tag{4}$$

At low Arp2/3, nucleation is roughly proportional to the product $A \times F_{\rm new}$, whereas at high Arp2/3 it is proportional to binding sites along new F-actin.

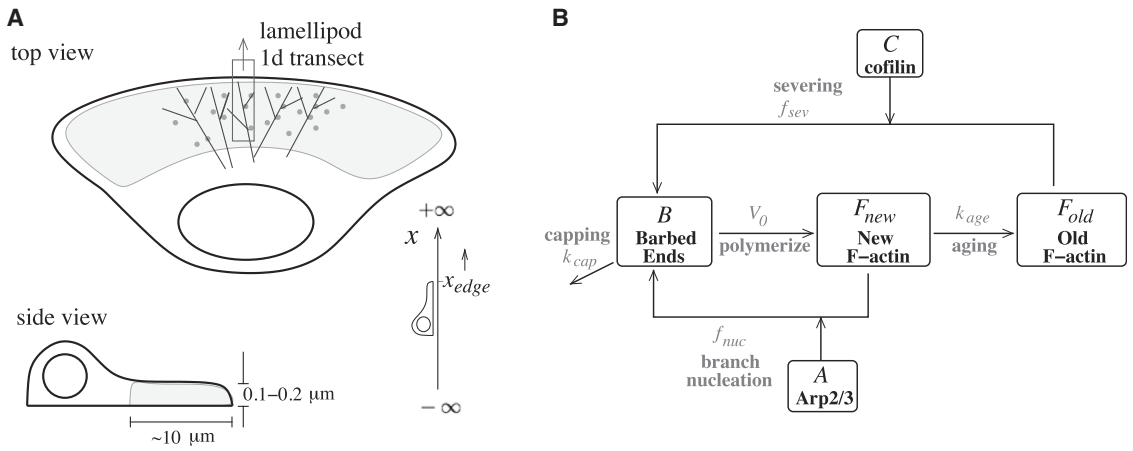

FIGURE 1 (*A*) Cell geometry showing a one-dimensional transect in top and side views (not to scale). Simulations span the region $x_L \le x \le x_{\rm edge}$, where $x_{\rm edge}$ is the cell edge and x_L is 4 μm into the cell. (*B*) Schematic diagram of the model. Cofilin severs old ADP-F-actin and Arp2/3 binds to new ATP-F-actin to generate barbed ends. These lead to polymerization of new F-actin, which ages into old F-actin.

Uncapped barbed ends, B, are generated by cofilin and Arp2/3 and disappear by capping (at rate k_{cap}, assumed constant), yielding

$$\frac{dB}{dt} = \kappa(f_{sev} + f_{nuc}) - k_{cap}\, B. \quad (5)$$

The constant κ is used for unit conversion from concentration to barbed-end density.

Spatially extended model

The geometry of our model consists of a thin and narrow transect as illustrated in Fig. 1 *A*. The thickness of the lamellipod ($<<1$ μm) and the assumed narrow width of the transect imply that there are no significant gradients in either of these dimensions. Thus, we reduce the problem to a one-dimensional domain $x \leq x_{edge}$, where x_{edge} denotes the location of the cell edge. We assume that both cofilin and Arp2/3 are locally activated at x_{edge}. We model the transient behavior seen in Mouneimne et al. (24), where an initially static cell starts to move after an EGF stimulation. Formulating a consistent moving boundary problem, i.e., correctly posing the boundary conditions to satisfy conservation laws, is nontrivial (see below and the Supporting Material). Furthermore, the accelerating cell edge makes simulation more challenging than that with the steady-state motion (8,30).

The equation for uncapped barbed-end density (units of *numbers*/μm^2) parallels Eq. 5, but with a term for motion toward the cell edge at the free-polymerization speed, V_0, assumed constant:

$$\frac{\partial B}{\partial t} = -\frac{\partial}{\partial x}(V_0 B) - k_{cap} B + \kappa(f_{sev} + f_{nuc}). \quad (6)$$

Uncapped barbed ends accumulating at the cell edge become pushing barbed ends, $B_p(t)$, that power cell protrusion by a thermal ratchet like mechanism (31). In the Supporting Material, we use conservation to derive the $B_p(t)$ equation (and boundary conditions),

$$\frac{dB_p}{dt} = (V_0 - V_{mb})B\big(x_{edge}, t\big) - k_{cap} B_p, \quad (7)$$

where V_{mb} is the cell-edge protrusion velocity. In turn, V_{mb} is determined by the pushing barbed ends. After Lacayo et al. (27), we assume that

$$V_{mb}\big(B_p\big) = V_0 \frac{B_p}{B_p + \phi \exp\big(\omega/B_p\big)}. \quad (8)$$

Equation 8 means that motility is initiated only when barbed ends have built up sufficiently, and that V_{mb} saturates to the free-polymerization speed V_0 at the high barbed-end density limit. The cell edge, x_{edge}, moves (dragging cytosol with it) according to

$$\frac{dx_{edge}}{dt} = V_{mb}\big(B_p(t)\big). \quad (9)$$

Free cofilin C is thereby transported by bulk flow toward the edge at velocity V_{mb}. It also diffuses (diffusion coefficient D_c), and is depleted by inactivation (rate k_c), and severing:

$$\frac{\partial C}{\partial t} = D_c \frac{\partial^2 C}{\partial x^2} - \frac{\partial}{\partial x}(V_{mb}\, C) - f_{sev}(C, F_{old}) - k_c\, C. \quad (10)$$

F-actin (units of length density μm/μm^2 = n/μm) is tethered to the substrate and does not diffuse. It satisfies Eqs. 1 and 2, which are now partial differential equations for $F_{new}(x,t)$ and $F_{old}(x,t)$. Active Arp2/3 is highly localized at and moves with the cell edge, bound to the WAVE2 complex. Arp2/3 is depleted as it nucleates barbed ends. Hence,

$$\frac{\partial A}{\partial t} = -\frac{\partial}{\partial x}(V_{mb}\, C) - f_{nuc}(A, F_{new}) - k_a\, A. \quad (11)$$

To avoid numerical issues, we implemented Eq. 11 with numerical diffusion (ϵA_{xx}), where ϵ is so small that active Arp2/3 is restricted to a thin region well within 0.1 μm of the cell edge, a compromise to allow for our continuum approximation model. (We also tested even smaller ϵ, where simulations are prohibitively slow; see the Supporting Material.) Very close to the membrane, active Arp2/3 can bind to new F-actin and nucleate barbed ends, according to $f_{nuc}(A,F_{new})$ from Eq. 4. A basal rate of Arp2/3 inactivation, k_a is included.

Local cofilin and Arp2/3 activation

At the cell membrane, cofilin is activated by PIP_2 hydrolysis after stimulation (6,24,28). We model this boundary condition with a transient inward edge flux (with $J_C(t) = 0$ for a resting cell). Arp2/3 is bound to the WAVE2 complex, and activated at the cell edge. Our boundary conditions are thus

$$\begin{aligned} \text{Cofilin}: \left[-D_c \frac{\partial C}{\partial x} + V_{mb}\, C \right]_{x = x_{edge}} &= -J_C(t), \\ \text{Arp2/3}: A\big(x_{edge}, t\big) &= A_{edge}(t) \end{aligned} \quad (12)$$

(here, $J_C(t)$, $A_{edge}(t) = 0$ at rest, > 0 during stimulation). In summary, EGF stimulation is depicted as a transient flux of active cofilin released into the cell interior, and a significant elevation of Arp2/3 at the edge. The relative times at which cofilin and Arp2/3 are activated might not coincide. We later investigate the effect of possible delay between these times.

Summaries of variables and functions are given in Table 1. Parameter values (see Table S1 in the Supporting Material) were taken from the literature or previous models (8,26,30),

TABLE 1 List of variables and functions used in the spatially extended model

	Definitions	Units	Equation
Variables			
x	Position	μm	
t	Time	s	
$F_{new}(x,t)$	New F-actin filament length density	$\mu m/\mu m^2$	1
$F_{old}(x,t)$	Old F-actin filament length density	$\mu m/\mu m^2$	2
$B(x,t)$	Barbed-end density	*numbers*/μm^2	6
$C(x,t)$	Cofilin concentration	μM	10
$A(x,t)$	Arp2/3 concentration	μM	11
$B_p(x,t)$	Number of pushing barbed ends per μm of cell edge	*numbers*/μm	7
$x_{edge}(t)$	Position of cell edge	μm	9
Functions			
$F_{sev}(C,F_{old})$	Cofilin severing function	μM/s	3
$F_{nuc}(A,F_{new})$	Arp2/3 nucleation function	μM/s	4
$V_{mb}(B_p)$	Membrane protrusion rate	μm/s	8
B_{prod}	Total barbed-end production per μm of cell edge	*numbers*/μm	15
S	Synergy between cofilin and Arp2/3	—	14

with sensitivity analysis discussed below. See also details in the Supporting Material.

RESULTS

Synergy in the well-mixed model

We first consider the well-mixed model (Eqs. 1–5) with basic parameter values (see Table S1) and resting/steady state as initial conditions. After a stimulus, the total number of barbed ends, B_{prod}, produced by cofilin and Arp2/3 integrated over time is

$$B_{prod} = \kappa \int_0^\infty (f_{sev} + f_{nuc})dt. \quad (13)$$

Barbed ends will be capped at rate k_{cap} (Eq. 5). For numerical simulations, we computed up to 60 s poststimulus, after which there is no further severing or nucleation (see Fig. S1 in the Supporting Material). Given cofilin and Arp2/3 stimuli amplitudes J_C and J_A, synergy is defined as in Ichetovkin et al. (5) and DesMarais et al. (11),

$$S(J_C,J_A) = \frac{B_{prod}(J_C,J_A)}{B_{prod}(J_C,0) + B_{prod}(0,J_A)}, \quad (14)$$

where $B_{prod}(X,Y)$ is total barbed ends generated by the given (cofilin, Arp2/3) stimuli. If cofilin and Arp2/3 act independently, then $S \approx 1$, whereas significant synergy implies $S > 1$.

Varying the step function heights J_C and J_A during the 10 s stimulus, we find that cofilin and Arp2/3 can each generate a large pulse of barbed ends (Fig. 2 *A*). The barbed-end production curves have two regimes:

1. A lower stimulus range with high sensitivity (a slight increase in activation leads to a much larger response), and
2. A higher stimulus range with low sensitivity (additional input results in a very modest further increase in barbed-end production).

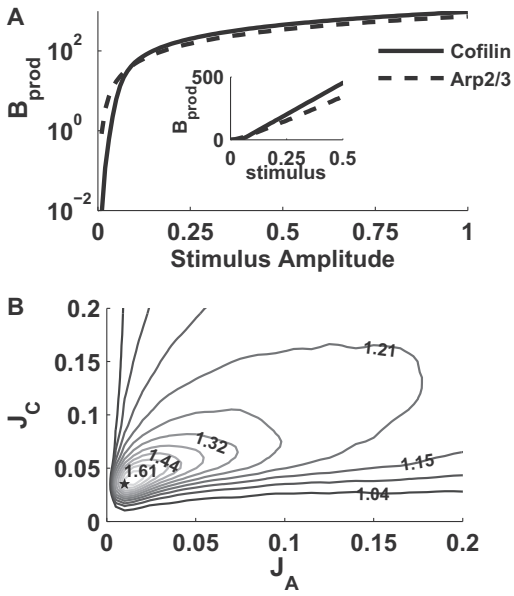

FIGURE 2 The well-mixed model (Eqs. 1–5). (*A*) Total number of barbed ends produced as a function of stimulus amplitude for cofilin alone (*solid*), and Arp2/3 alone (*dashed*). (*Inset*) Same plot on a linear scale. (*B*) Synergy S of cofilin and Arp2/3 as in Eq. 14. Maximum synergy (*star*) at $(J_C, J_A) = (0.036, 0.012)$ μM/s. Parameter values as in Table S1 in the Supporting Material. Steady-state initial conditions: $A(0) = 0$, $C(0) = 0$, $B(0) = 0$, $F_{new}(0) = J_f/k_{age}$, and $F_{old} = J_f/k_{deg}$. Cofilin and Arp2/3 were activated simultaneously for 10 s.

In the presence of both cofilin and Arp2/3 (Fig. 2 *B*), a high synergy of ~1.8 is only observed in the low stimulus range with high sensitivity. In this regime, cofilin and Arp2/3 produce very few barbed ends on their own but the total barbed-end production is very sensitive to additional stimulation, so that, by acting together, cofilin and Arp2/3 synergistically produce many more barbed ends. However, even with synergy, the level of barbed ends produced was still far too low (maximum value of $<2/\mu m^2$ at maximal synergy, graph not shown) corresponding to a protrusion rate close to zero in the spatially extended model (see Eq. 8). Higher stimulation yields a low level of synergy (~1.2 or less), much too low to account for in vitro experimental observation of 2× or higher synergy during simultaneous cofilin and Arp2/3 activation (5). We later show that this limitation is not observed in the spatially extended version of the model, highlighting the importance of spatial localization.

Results of the spatially extended model

Spatiotemporal dynamics in response to simultaneous cofilin and Arp2/3 activation are shown in Fig. 3 and Movie S1 (see the Supporting Material). Close to the cell edge, the

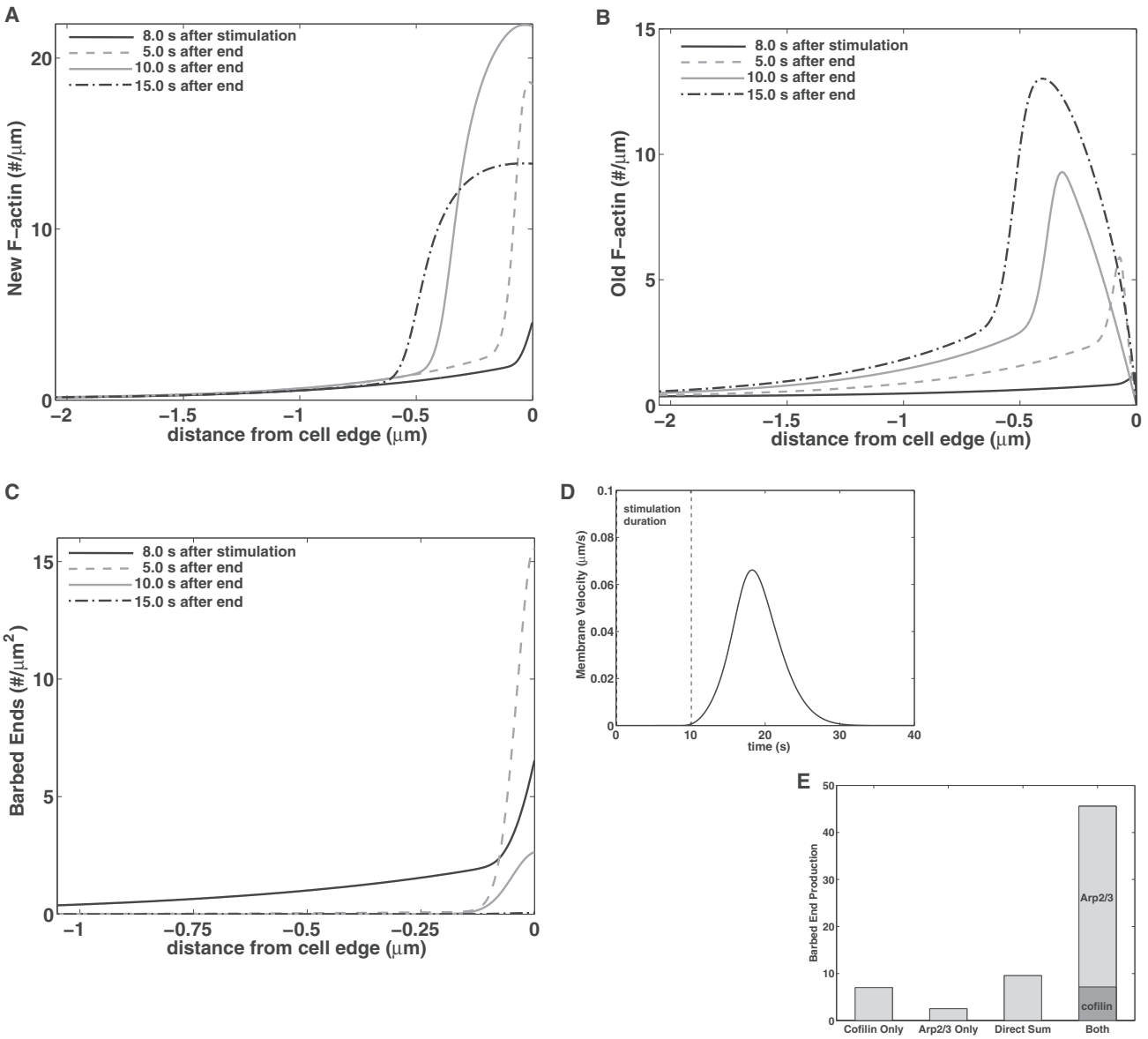

FIGURE 3 The spatial model with simultaneous activation of cofilin and Arp2/3 for 10 s ($J_C = 1.6\ \mu M \times \mu m/s$, $A_{edge} = 44\ \mu M$ for $0.1 \leq t \leq 10.1$ s; see boundary conditions in Eq. 12). (*A–C*) Profiles of new F-actin, and old F-actin, and barbed ends during stimulation (at 8 s) and at 5, 10, and 15 s after the end of stimulus. (*D*) The protrusion rate V_{mb} as a function of time. (*E*) Total barbed-end production obtained using cofilin alone; Arp2/3 alone; the expected barbed ends without synergy (direct sum); and in the presence of both. The barbed ends produced by cofilin ($\int\int F_{sev}\, dx\, dt$) and by Arp2/3 ($\int\int F_{nuc}\, dx\, dt$) are shown.

concentrations of active cofilin and Arp2/3 increase rapidly within the first 5 s of stimulation, then remain relatively fixed until $t = 10$ s (see Movie S1) at the cell edge. During this period, active cofilin is elevated throughout the domain (4 μm). With ~2 s delay, barbed ends accumulate (Fig. 3 *C*) with peak density at the cell edge. The pushing barbed ends, B_p, reach their maximal density at ~8 s poststimulus. Edge protrusion, at a rate V_{mb} (Eq. 8 and Fig. 3 *D*), leaves behind F-actin (Fig. 3, *A* and *B*) whose density peaks ~1 μm from the cell edge, consistent with recent data in Bravo-Cordero et al. (32). After the end of stimulation, cofilin and Arp2/3 decay, whereas F-actin polymerization continues for 10–20 s. Because capping eliminates barbed ends, the system gradually returns to its basal steady state.

In Fig. 3 *E*, we show total barbed ends that are produced by cofilin and Arp2/3 each acting alone, then the direct sum, and then the synergistic production. When both cofilin and Arp2/3 are present, their respective contribution is computed by integrating f_{sev} and f_{nuc}, respectively. Spatial distribution of severing (f_{sev}) and nucleation (f_{nuc}) rates over time are shown in Fig. S2. The spatial extent of cofilin (~1 μm) severing is an order-of-magnitude larger than that of Arp2/3 nucleation in our model, though both peak at

the cell edge. We find that ~84% of total barbed ends are produced by Arp2/3 nucleation, with only ~16% by cofilin. Importantly, cofilin primes the system by initially generating barbed ends from old filaments.

High synergy and large barbed ends peak in the spatial model

The total barbed-end production in the spatial model is computed by integrating over space and time,

$$B_{\text{prod}} = \kappa \int_0^{\infty} \int_{-\infty}^{x_{\text{edge}}} (f_{\text{sev}} + f_{\text{nuc}}) dx\, dt. \qquad (15)$$

Synergy is then computed according to Eq. 14 as before, with A_{edge} replacing J_A in Eq. 14.

Barbed-end production in the presence of either cofilin or Arp2/3 alone is shown in Fig. 4 *A*. Although the Arp2/3 curve resembles that of the well-mixed system (Fig. 2 *A*), the cofilin production curve increases more gradually for low and mid-range cofilin stimulation. We attribute this to the fact that cofilin is activated at the cell edge, but severs old F-actin that is concentrated farther away (~1 μm from the edge). There is a wide stimulus range over which barbed-end production is both sufficiently large and highly sensitive to additional stimulation. This then allows for simultaneously high synergy as well as large production of barbed ends as shown in Fig. 4 *B*.

The dependence of synergy and maximal protrusion rate on both cofilin (J_C) and Arp2/3 (A_{edge}) activation at the cell edge is shown in Fig. 4 *B*. High synergy (up to ~9.9) occurs for $1 < J_C < 3$ μM $\times$ μm/s, provided A_{edge} is high ($250 < A_{\text{edge}} < 400$ μM). In the high synergy regime, a large pulse of barbed ends occurs, leading to fast protrusion (V_{mb} ~ 0.28 μm/s at maximum synergy).

High synergy is obtained when barbed ends due to cofilin grow into new F-actin, which facilitates Arp2/3 nucleation. DesMarais et al. (11) found that the ratio of barbed ends produced by cofilin and by Arp2/3 (when each acts alone) is ~2:1. This experimental result constrains the values of J_C and A_{edge} to $1.6 < J_C < 1.8$ μM•μm/s and $40 < A_{\text{edge}} < 60$ μM. We use this range in the rest of the article and find that this leads to model predictions that are most consistent with the experimental finding of DesMarais et al. (11). Within this range, a sufficiently high protrusion rate (0.05–0.2 μm/s), synergy of 4–5, and barbed-end production ratio of 2.5–3 (cofilin to Arp2/3 when each acts alone) were obtained (also see Fig. 3 *E*).

Relative timing of cofilin and Arp2/3 activation

Experiments on EGF stimulation of mammary carcinoma cells indicate that Arp2/3 activation occurs ~10–20 s later than cofilin activation (11,24). The active cofilin is released from membrane lipid PIP_2 after hydrolysis by PLC (6,33), whereas Arp2/3 is activated by the Cdc42-regulated WAVE2 (19,34,35), so distinct signaling pathways are at play. In the simulations so far, we assumed that cofilin and Arp2/3 are activated simultaneously. Now, we consider the effect of this relative Arp2/3 delay on our predictions.

In Fig. 5 *A*, we show how synergy changes as Arp2/3 activation is delayed relative to cofilin activation. During a delay τ, cofilin-generated barbed ends extend by $V_0\tau$, forming new filament density ($V_0\tau B$) for Arp2/3 to bind. Capping eventually eliminates these barbed ends, resulting in the nonmonotonic relationship shown. Synergy (*solid curve*) nearly doubles from $S = 4.7$ (no delay) to a maximum of

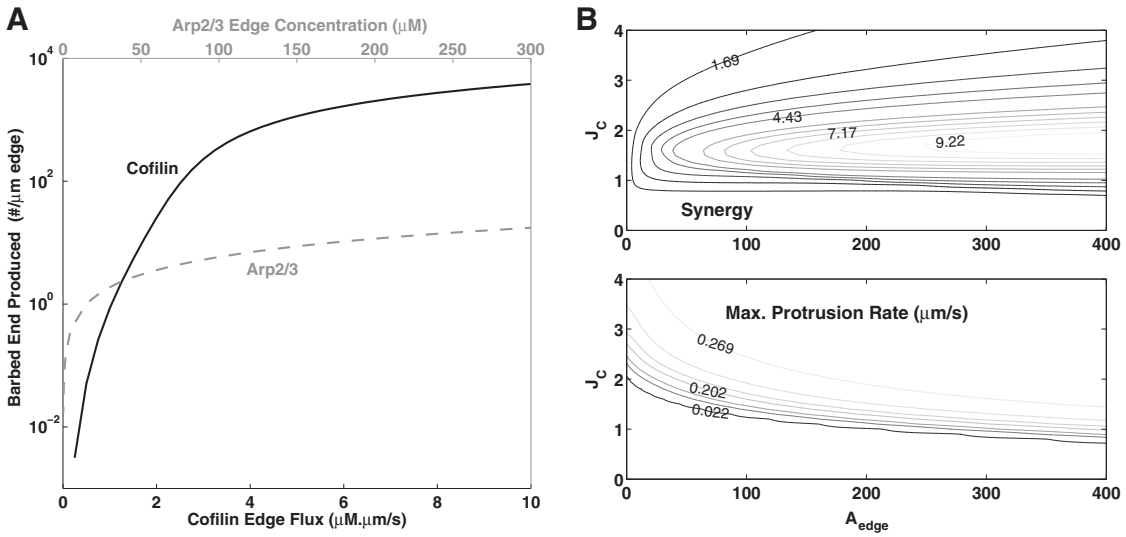

FIGURE 4 Barbed ends and synergy in the spatial model. (*A*) Total barbed ends (Eq. 15) produced by cofilin (*solid*) or Arp2/3 (*gray*) alone. (*B*) Synergy (*top*) and maximum protrusion rate V_{max} (*bottom*) for varying cofilin flux, J_C, and Arp2/3 edge concentration, A_{edge} (10 s simultaneous activation as in Fig. 3).

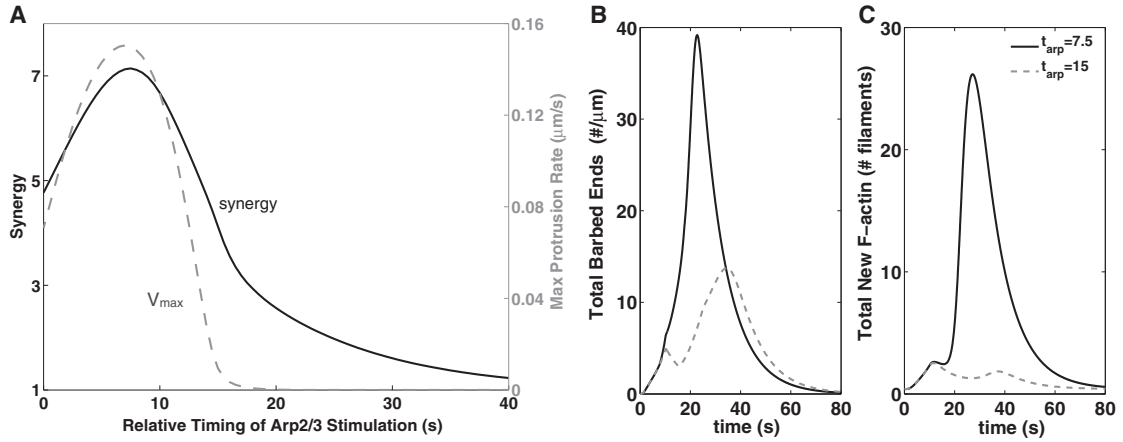

FIGURE 5 A delay in Arp2/3 activation affects cofilin-Arp2/3 synergy. (*A*) Synergy (*solid*) obtained as the relative timing of Arp2/3 activation is varied. The corresponding maximum protrusion rate is also shown (*gray curve*, axis on the *right*). (*B* and *C*) Comparison of barbed-end production when Arp2/3 is introduced at $t_a = 7.5$ s (*dashed gray curve*) and at 15 s (*gray curve*), after cofilin activation. (*B*) Actin barbed ends (total barbed ends $\int B(x,t)dx + B_p(t)$); (*C*) new F-actin ($\int F_{\text{new}}\,dx$). ($J_C = 1.6\ \mu\text{M} \times \mu\text{m/s}$; $A_{\text{edge}} = 44\ \mu\text{M}$, as in Fig. 3; 10 s cofilin ($0 < t < 10$) and Arp2/3 stimuli with variation in the timing of Arp2/3 activation.)

$S = 7.1$, when Arp2/3 activation is delayed by $t_{\text{arp}} \sim 7.5$ s. The maximal protrusion rate (*dashed gray curve*) increases by >50% over the same interval. This indicates that the ultimate output—cell protrusion—is affected by the relative timing of cofilin and Arp2/3 activation.

In Fig. 5, *B* and *C*, we plot the total barbed ends and new F-actin over time, for two values of t_{arp}. For $t_{\text{arp}} = 7.5$ s, barbed ends created by cofilin severing have generated enough new F-actin to optimally prime the system for Arp2/3 action. As a result, we see a larger peak of barbed ends being generated, accompanied by a higher protrusion rate. For $t_{\text{arp}} = 15$ s, some of that F-actin has already aged, so a smaller burst of barbed ends and lower protrusion rate is obtained. However, this yields two distinct peaks of barbed ends, as previously observed by Mouneimne et al. (24).

Filament protection by tropomyosin

Tropomyosin density increases from the cell edge inwards (36), and competes with cofilin for actin binding (37). We asked how this competition would affect our model results. To avoid significant expansion of the minimal model, we simply assumed that tropomyosin binding removes available cofilin binding sites on old F-actin. To do so, we modified the removal term, k_{deg} in Eq. 2 to $k_{\text{deg}}(x) = k_{\text{deg}} - d_T(x)$, with $d_T(x)$ a linear gradient, as in DesMarais et al. (36). We also included a class of tropomyosin-protected filaments, F_{tm} (details in the Supporting Material). We found that tropomyosin decreases barbed-end production by cofilin and restricts its activity more sharply, within ~0.5 μm, toward the cell edge (see Fig. S3). Inclusion of tropomyosin does not qualitatively change our synergy results. We still obtain a cofilin barbed-end production curve with wide sensitive region, as before.

Binding to old versus new filaments

Recent data from Ti et al. (38) suggests that Arp2/3 binds to old (ADP-Pi and ADP) F-actin with similar kinetics, and higher affinity than to new (ATP) F-actin (although possibly without branching). To investigate how this would affect synergy, we modified the previous Arp2/3 binding term to

$$f_{\text{nuc}}(A, F_{\text{new}}, F_{\text{old}}) = (1-\alpha)k_{\text{nuc}}\frac{A}{K_m + A}\,\ell F_{\text{new}} + \alpha k_{\text{nuc}}\frac{A}{K_m + A}\,\ell F_{\text{old}} \qquad (16)$$

for $0 \le \alpha \le 1$ as the preferential binding of Arp2/3 to new ($\alpha \sim 0$) versus old ($\alpha \sim 1$) F-actin.

As shown in Fig. 6, $\alpha = 0$ results in many barbed ends and a large protrusion rate. Larger α leads to lower Arp2/3 nucleation (and lower protrusion rate, *dashed curve*, Fig. 6 *A*). Larger α also lowers the synergy (*solid curve*, Fig. 6 *A*) and the peak of barbed ends produced (Fig. 6 *B*) but does not eliminate it: barbed ends created by cofilin still accelerate the substrate on which Arp2/3 can act. These results suggest that Arp2/3 binding to old F-actin has at most minor effect, because the narrow localization of Arp2/3 at the cell edge provides little overlap with old F-actin further into the cell. Overall, this agrees with results of a well-mixed model by Carlsson (39), who found Arp2/3-cofilin synergy only if Arp2/3 binds exclusively to new filaments.

We similarly considered the effect of cofilin binding (at low affinity) and severing of new F-actin, as in Blanchoin et al. (14) and Chan et al. (40). In the Supporting Material, we show that this model modification leads to scarcely any change: only a slight increase in barbed-end production and a drop in synergy. Note that we did not consider other putative cofilin roles such as accelerating phosphate release from

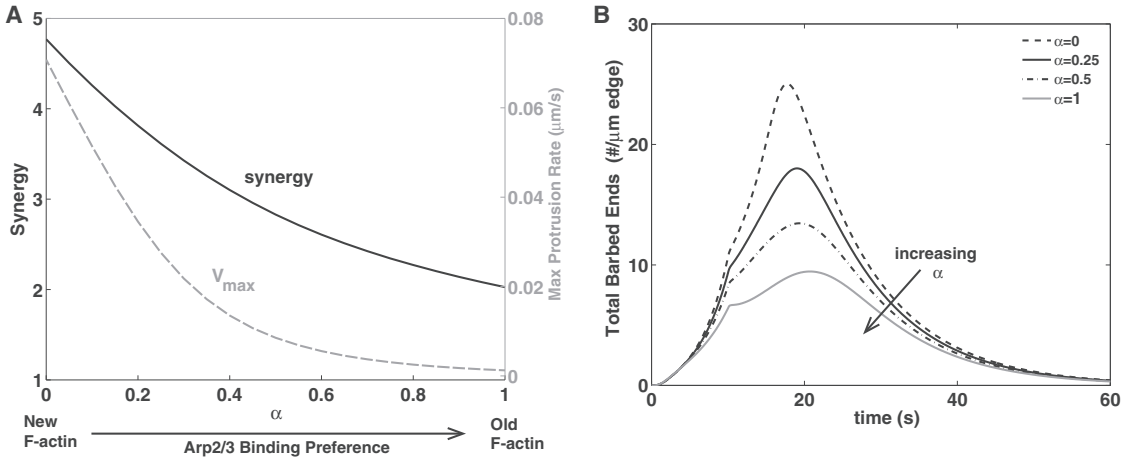

FIGURE 6 Effect of Arp2/3 binding preference to new ATP-F-actin versus old ADP-F-actin, depicted by α in Eq. 16. (*A*) Maximum protrusion rate V_{max} (in *gray dashed line*) and synergy (in *solid line*) versus α. As in Fig. 3, $J_C = 1.6\ \mu M \times \mu m/s$ and $A_{edge} = 44\ \mu M$, simultaneous cofilin and Arp2/3 activation for 10 s, but with Arp2/3 barbed-end production rate defined in Eq. 16. (*B*) Time course of total number of barbed ends ($\int B(x,t)dx + B_p(t)$) for $\alpha = 0$, 0.25, 0.5, and 1.

F-actin, which promotes Arp2/3 dissociation and resultant filament debranching (14).

Parameter sensitivity

To check the sensitivity of our results, we varied key model parameters. Results are detailed extensively in the Supporting Material and briefly summarized here.

Filament aging

Some in vitro studies report slower rates of transition to ADP-actin (16–18), though other studies estimate the transition to ADP-actin to be 10 times faster in vivo, due to cofilin (3,13,14). We asked how varying the filament aging rate, k_{age}, would affect our results. Briefly, when cofilin and Arp2/3 act together, barbed-end production increases monotonically with k_{age} (see the Supporting Material). However, maximal synergy occurs when $k_{age} \approx 0.12$/s. Interestingly, this closely coincides with the value of k_{age} reported in vivo.

Barbed-end capping and rate of growth

We found that faster capping (larger k_{cap}) leads to a decrease in both barbed-end production and synergy whereas faster polymerization (higher V_0) leads to a larger burst of barbed-end production as well as an increase in synergy. In the presence of cofilin and Arp2/3 alone, an increase in k_{cap} leads to little change in barbed-end production but lead to a larger difference when cofilin and Arp2/3 are both present and working synergistically (see the Supporting Material for details).

DISCUSSION

In this article, we explored synergy between cofilin and Arp2/3 in creating new barbed ends. Our model includes F-actin aging, capping, and severing by cofilin, as in Ditlev et al. (10) and Stuhrmann et al. (41) but not monomer recycling, nor the rare spontaneous nucleation of actin filaments from monomers. The model was motivated by data for transient responses of EGF-stimulated mammary carcinoma cells (11). There, cofilin is released from the membrane and its activity is focused in a zone ~1 μm of the cell edge. Our model would apply (with suitable modifications) to other cells in which such release takes place, provided the cell-edge environment leads to a dominant filament-severing role of cofilin. Arp2/3 activity is restricted to a much smaller zone at the cell membrane (<0.1 μm). The maximum barbed-end density at the cell edge emerges as a model prediction that depends on biochemical rates, spatial localization of Arp2/3 and cofilin, and their relative timing.

Our model goes beyond Tania et al. (28), where a coarse spatial representation (two well-mixed compartments) was used. There, we considered multiple cofilin states in finer detail, but not the interaction with Arp2/3. Even so, we already noted that the peak of barbed ends depends on events occurring close to the cell membrane. Here we reduced the detail of the cofilin cycle, but included its interplay with Arp2/3 in both well-mixed and spatially distributed settings. In the well-mixed model, synergy is significant only at low cofilin and Arp2/3 activities and does not correlate well with barbed ends generated (Fig. 2). We note that correct formulation of the moving boundary problem for the cell edge, a challenging modeling issue, is an important feature of our model (see the Supporting Material).

Our spatially distributed model demonstrates a wide range of cofilin and Arp2/3 activity consistent with synergy and significant production of barbed ends. Synergy is accentuated if cofilin activity precedes Arp2/3 activity, because cofilin primes the system with new F-actin on which Arp2/3 can act. Hence, our model points to the fact that both spatial distribution and relative timing of cofilin and Arp2/3 activation are important determinants of synergy.

We carried out parameter sensitivity analysis, and modified several key model assumptions. For example, we showed that if cofilin severs new (ATP) F-actin then barbed-end production increases, but synergy decreases. In contrast, the binding of Arp2/3 to old F-actin has little effect, because the two have widely divergent spatial localizations.

We showed that by removing old F-actin binding sites, tropomyosin competes with and localizes cofilin activity (36,37) (see the Supporting Material). In this round of modeling, we did not, however, include a fully dynamic tropomyosin variable, nor its effect on Arp2/3 (42,43). Our preliminary results on tropomyosin suggest that this could be a fruitful future study.

We here assumed constant polymerization rate, $V_0 = 0.3\ \mu$m/s, for barbed ends away from the membrane, neglecting G-actin availability. Cofilin is known to also depolymerize actin and disassemble old filaments, allowing for G-actin monomers to be recycled (44–46). This monomer-recycling would increase available ATP-G-actin, speeding polymerization of ATP-F-actin, and enhancing the synergy between cofilin and Arp2/3. Using a realistic three-dimensional geometry, Novak et al. (9) found that F-actin disassembly at the rear and rapid polymerization at the front creates a concentration gradient that transports G-actin to the cell edge where it is being used up, thereby sustaining polymerization. G-actin recycling/sequestration by cofilin and other regulators (e.g., profilin and thymosin) has been previously considered in detail (8,10,47). Here, we focused on the complementary hypothesis of synergy via barbed-end production, which has yet to receive modeling attention. Incorporating G-actin into future versions of the model could allow us to study longer periods of activation where G-actin depletion becomes more significant.

Whereas some recent studies focused on the physical details of cofilin binding, individual filament geometry, filament bending (48), and severing (29,49,50) as well as its effect on nucleotide state of F-actin (50,51), here we focused solely on its role in creating new barbed ends by severing preexisting filaments (5,11,52). We have not considered the roles of other proteins such as Aip1 and coronin in regulating cofilin activity (53), nor profilin or thymosin that sequester G-actin or compete for binding. Finally, we simulated only low cofilin concentrations where severing, rather than de novo actin nucleation, occurs (54). Such omissions are limitations of our simplified continuum model, but keep its complexity manageable.

Our models make predictions about detailed spatial distributions of barbed-end and F-actin density that are experimentally testable. Although the cofilin-Arp2/3 synergy may well exist in a variety of cell types, the most extensive data sets are found in mammary carcinoma cells (11,24,36). The profiles we obtained agree qualitatively with spatial measurements in these articles. So far, such data were gathered at very coarse temporal resolution. Better time-resolution experiments would allow more direct quantitative comparisons. Experiments in which either Arp2/3 or cofilin are selectively inhibited would allow comparison to our predictions for synergy. Further, tests that manipulate monomer availability (hence V_0), capping rates (hence k_{cap}), or filament aging (k_{age}) could be compared with predictions we have made above.

SUPPORTING MATERIAL

Eight figures, one table, three movies, references (55–59) and supplemental information are available at http://www.biophysj.org/biophysj/supplemental/S0006-3495(13)01033-3.

We are grateful to Eric Cytrynbaum, Jun Allard, and participants of a Banff International Research Station workshop, August 2011, for discussions.

This research was supported by a subcontract (to L.E.-K.) from the National Institutes of Health (grant No. R01 GM086882) to Anders Carlsson, Washington University, and by a Natural Sciences and Engineering Research Council of Canada discovery grant (to L.E.-K.). J.C. is funded by National Institutes of Health grant No. CA150344.

REFERENCES

1. Bailly, M., F. Macaluso, …, J. S. Condeelis. 1999. Relationship between Arp2/3 complex and the barbed ends of actin filaments at the leading edge of carcinoma cells after epidermal growth factor stimulation. *J. Cell Biol.* 145:331–345.
2. Mullins, R. D., J. A. Heuser, and T. D. Pollard. 1998. The interaction of Arp2/3 complex with actin: nucleation, high affinity pointed end capping, and formation of branching networks of filaments. *Proc. Natl. Acad. Sci. USA.* 95:6181–6186.
3. Pollard, T. D., L. Blanchoin, and R. D. Mullins. 2000. Molecular mechanisms controlling actin filament dynamics in nonmuscle cells. *Annu. Rev. Biophys. Biomol. Struct.* 29:545–576.
4. Pollard, T. D., and G. G. Borisy. 2003. Cellular motility driven by assembly and disassembly of actin filaments. *Cell.* 112:453–465.
5. Ichetovkin, I., W. Grant, and J. Condeelis. 2002. Cofilin produces newly polymerized actin filaments that are preferred for dendritic nucleation by the Arp2/3 complex. *Curr. Biol.* 12:79–84.
6. van Rheenen, J., X. Song, …, J. S. Condeelis. 2007. EGF-induced PIP2 hydrolysis releases and activates cofilin locally in carcinoma cells. *J. Cell Biol.* 179:1247–1259.
7. Wang, W., R. Eddy, and J. Condeelis. 2007. The cofilin pathway in breast cancer invasion and metastasis. *Nat. Rev. Cancer.* 7:429–440.
8. Mogilner, A., and L. Edelstein-Keshet. 2002. Regulation of actin dynamics in rapidly moving cells: a quantitative analysis. *Biophys. J.* 83:1237–1258.
9. Novak, I. L., B. M. Slepchenko, and A. Mogilner. 2008. Quantitative analysis of G-actin transport in motile cells. *Biophys. J.* 95:1627–1638.
10. Ditlev, J. A., N. M. Vacanti, …, L. M. Loew. 2009. An open model of actin dendritic nucleation. *Biophys. J.* 96:3529–3542.
11. DesMarais, V., F. Macaluso, …, M. Bailly. 2004. Synergistic interaction between the Arp2/3 complex and cofilin drives stimulated lamellipod extension. *J. Cell Sci.* 117:3499–3510.
12. Mahaffy, R. E., and T. D. Pollard. 2006. Kinetics of the formation and dissociation of actin filament branches mediated by Arp2/3 complex. *Biophys. J.* 91:3519–3528.
13. Blanchoin, L., and T. D. Pollard. 1999. Mechanism of interaction of *Acanthamoeba* actophorin (ADF/Cofilin) with actin filaments. *J. Biol. Chem.* 274:15538–15546.

14. Blanchoin, L., T. D. Pollard, and R. D. Mullins. 2000. Interactions of ADF/cofilin, Arp2/3 complex, capping protein and profilin in remodeling of branched actin filament networks. *Curr. Biol.* 10:1273–1282.
15. Blanchoin, L., and T. D. Pollard. 2002. Hydrolysis of ATP by polymerized actin depends on the bound divalent cation but not profilin. *Biochemistry.* 41:597–602.
16. Carlier, M. F., and D. Pantaloni. 1986. Direct evidence for ADP-Pi-F-actin as the major intermediate in ATP-actin polymerization. Rate of dissociation of Pi from actin filaments. *Biochemistry.* 25:7789–7792.
17. Melki, R., S. Fievez, and M.-F. Carlier. 1996. Continuous monitoring of Pi release after nucleotide hydrolysis in actin or tubulin assembly using 2-amino-6-mercapto-7-methylpurine ribonucleoside and purine-nucleoside phosphorylase as an enzyme-linked assay. *Biochemistry.* 35: 12038–12045.
18. Jégou, A., T. Niedermayer, …, G. Romet-Lemonne. 2011. Individual actin filaments in a microfluidic flow reveal the mechanism of ATP hydrolysis and give insight into the properties of profilin. *PLoS Biol.* 9:e1001161.
19. Sarmiento, C., W. Wang, …, J. Condeelis. 2008. WASP family members and formin proteins coordinate regulation of cell protrusions in carcinoma cells. *J. Cell Biol.* 180:1245–1260.
20. Lai, F. P., M. Szczodrak, …, K. Rottner. 2008. Arp2/3 complex interactions and actin network turnover in lamellipodia. *EMBO J.* 27: 982–992.
21. Welch, M. D., and R. D. Mullins. 2002. Cellular control of actin nucleation. *Annu. Rev. Cell Dev. Biol.* 18:247–288.
22. Bamburg, J. R., and O. P. Wiggan. 2002. ADF/cofilin and actin dynamics in disease. *Trends Cell Biol.* 12:598–605.
23. Bravo-Cordero, J. J., M. A. O. Magalhaes, …, J. Condeelis. 2013. Functions of cofilin in cell locomotion and invasion. *Nat. Rev. Mol. Cell Biol.* 14:405–415.
24. Mouneimne, G., L. Soon, …, J. Condeelis. 2004. Phospholipase C and cofilin are required for carcinoma cell directionality in response to EGF stimulation. *J. Cell Biol.* 166:697–708.
25. Zigmond, S. H. 2004. Formin-induced nucleation of actin filaments. *Curr. Opin. Cell Biol.* 16:99–105.
26. Marée, A. F., A. Jilkine, …, L. Edelstein-Keshet. 2006. Polarization and movement of keratocytes: a multiscale modeling approach. *Bull. Math. Biol.* 68:1169–1211.
27. Lacayo, C. I., Z. Pincus, …, J. A. Theriot. 2007. Emergence of large-scale cell morphology and movement from local actin filament growth dynamics. *PLoS Biol.* 5:e233.
28. Tania, N., E. Prosk, …, L. Edelstein-Keshet. 2011. A temporal model of cofilin regulation and the early peak of actin barbed ends in invasive tumor cells. *Biophys. J.* 100:1883–1892.
29. De La Cruz, E. M., and D. Sept. 2010. The kinetics of cooperative cofilin binding reveals two states of the cofilin-actin filament. *Biophys. J.* 98:1893–1901.
30. Dawes, A. T., G. Bard Ermentrout, …, L. Edelstein-Keshet. 2006. Actin filament branching and protrusion velocity in a simple 1D model of a motile cell. *J. Theor. Biol.* 242:265–279.
31. Mogilner, A., and G. Oster. 1996. Cell motility driven by actin polymerization. *Biophys. J.* 71:3030–3045.
32. Bravo-Cordero, J. J., V. P. Sharma, …, L. Hodgson. 2013. Spatial regulation of RhoC activity defines protrusion formation in migrating cells. *J. Cell Sci.* 126:3356–3369.
33. van Rheenen, J., J. Condeelis, and M. Glogauer. 2009. A common cofilin activity cycle in invasive tumor cells and inflammatory cells. *J. Cell Sci.* 122:305–311.
34. Millard, T. H., S. J. Sharp, and L. M. Machesky. 2004. Signaling to actin assembly via the WASP (Wiskott-Aldrich syndrome protein) family proteins and the Arp2/3 complex. *Biochem. J.* 380:1–17.
35. El-Sibai, M., P. Nalbant, …, J. M. Backer. 2007. Cdc42 is required for EGF-stimulated protrusion and motility in MTLn3 carcinoma cells. *J. Cell Sci.* 120:3465–3474.
36. DesMarais, V., I. Ichetovkin, …, S. E. Hitchcock-DeGregori. 2002. Spatial regulation of actin dynamics: a tropomyosin-free, actin-rich compartment at the leading edge. *J. Cell Sci.* 115:4649–4660.
37. Ono, S., and K. Ono. 2002. Tropomyosin inhibits ADF/cofilin-dependent actin filament dynamics. *J. Cell Biol.* 156:1065–1076.
38. Ti, S. C., C. T. Jurgenson, …, T. D. Pollard. 2011. Structural and biochemical characterization of two binding sites for nucleation-promoting factor WASP-VCA on Arp2/3 complex. *Proc. Natl. Acad. Sci. USA.* 108:E463–E471.
39. Carlsson, A. E. 2006. Stimulation of actin polymerization by filament severing. *Biophys. J.* 90:413–422.
40. Chan, C., C. C. Beltzner, and T. D. Pollard. 2009. Cofilin dissociates Arp2/3 complex and branches from actin filaments. *Curr. Biol.* 19:537–545.
41. Stuhrmann, B., F. Huber, and J. Käs. 2011. Robust organizational principles of protrusive biopolymer networks in migrating living cells. *PLoS ONE.* 6:e14471.
42. Blanchoin, L., T. D. Pollard, and S. E. Hitchcock-DeGregori. 2001. Inhibition of the Arp2/3 complex-nucleated actin polymerization and branch formation by tropomyosin. *Curr. Biol.* 11:1300–1304.
43. Cooper, J. A. 2002. Actin dynamics: tropomyosin provides stability. *Curr. Biol.* 12:R523–R525.
44. Carlier, M.-F., V. Laurent, …, D. Pantaloni. 1997. Actin depolymerizing factor (ADF/cofilin) enhances the rate of filament turnover: implication in actin-based motility. *J. Cell Biol.* 136:1307–1322.
45. Bamburg, J. R. 1999. Proteins of the ADF/cofilin family: essential regulators of actin dynamics. *Annu. Rev. Cell Dev. Biol.* 15:185–230.
46. Pantaloni, D., C. Le Clainche, and M.-F. Carlier. 2001. Mechanism of actin-based motility. *Science.* 292:1502–1506.
47. Rubinstein, B., K. Jacobson, and A. Mogilner. 2005. Multiscale two-dimensional modeling of a motile simple-shaped cell. *Multiscale Model Simul.* 3:413–439.
48. Murrell, M. P., and M. L. Gardel. 2012. F-actin buckling coordinates contractility and severing in a biomimetic actomyosin cortex. *Proc. Natl. Acad. Sci. USA.* 109:20820–20825.
49. Roland, J., J. Berro, …, J.-L. Martiel. 2008. Stochastic severing of actin filaments by actin depolymerizing factor/cofilin controls the emergence of a steady dynamical regime. *Biophys. J.* 94:2082–2094.
50. McCullough, B. R., E. E. Grintsevich, …, E. M. De La Cruz. 2011. Cofilin-linked changes in actin filament flexibility promote severing. *Biophys. J.* 101:151–159.
51. Suarez, C., J. Roland, …, L. Blanchoin. 2011. Cofilin tunes the nucleotide state of actin filaments and severs at bare and decorated segment boundaries. *Curr. Biol.* 21:862–868.
52. Du, J., and C. Frieden. 1998. Kinetic studies on the effect of yeast cofilin on yeast actin polymerization. *Biochemistry.* 37:13276–13284.
53. Kueh, H. Y., G. T. Charras, …, W. M. Brieher. 2008. Actin disassembly by cofilin, coronin, and Aip1 occurs in bursts and is inhibited by barbed-end cappers. *J. Cell Biol.* 182:341–353.
54. Andrianantoandro, E., and T. D. Pollard. 2006. Mechanism of actin filament turnover by severing and nucleation at different concentrations of ADF/cofilin. *Mol. Cell.* 24:13–23.
55. Svitkina, T. M., and G. G. Borisy. 1999. Arp2/3 complex and actin depolymerizing factor/cofilin in dendritic organization and treadmilling of actin filament array in lamellipodia. *J. Cell Biol.* 145:1009–1026.
56. De La Cruz, E. M., A. Mandinova, …, T. D. Pollard. 2000. Polymerization and structure of nucleotide-free actin filaments. *J. Mol. Biol.* 295:517–526.
57. Nishida, E., S. Maekawa, and H. Sakai. 1984. Cofilin, a protein in porcine brain that binds to actin filaments and inhibits their interactions with myosin and tropomyosin. *Biochemistry.* 23:5307–5313.
58. Abraham, V. C., V. Krishnamurthi, …, F. Lanni. 1999. The actin-based nanomachine at the leading edge of migrating cells. *Biophys. J.* 77: 1721–1732.
59. Wegner, A., and K. Ruhnau. 1988. Rate of binding of tropomyosin to actin filaments. *Biochemistry.* 27:6994–7000.

Modeling the Synergy of Cofilin and Arp2/3 in Lamellipodial Protrusive Activity

Nessy Tania[a,b], John Condeelis[c], and Leah Edelstein-Keshet[a1]

[a]Department of Mathematics,
University of British Columbia, Vancouver, BC V6T 1Z2, Canada

[b] Department of Mathematics and Statistics,
Smith College, Northampton, MA 01063

[c]Department of Anatomy and Structural Biology,
Gruss Lipper Biophotonics Center,
Albert Einstein College of Medicine of Yeshiva University, Bronx, NY 10461

[1]Corresponding author
Email: keshet@math.ubc.ca

Contents

1 Well-Mixed Model

Below we list the full model equations for the well mixed model as discussed in the main paper and simulation results showing response to a transient stimulation.

1.1 Equations

Within a transect of the lamellipod, we keep track of the length density of F-actin filaments (new ATP-F-actin, F_{new}, and old ADP-F-actin, F_{old}) and the corresponding barbed end density B, as well as the concentrations of active cofilin, C, and Arp2/3, A. The definitions and values of parameters are given in Table S1.

New F-actin

$$\frac{dF_{new}}{dt} = J_f - k_{age}\, F_{new} + V_0\, B\,, \tag{S1}$$

Old F-actin

$$\frac{dF_{old}}{dt} = k_{age}\, F_{new} - k_{deg}\, F_{old}\,, \tag{S2}$$

Barbed Ends

$$\frac{dB}{dt} = \kappa(f_{sev}(C, F_{old}) + f_{nuc}(A, F_{new})) - k_{cap} B\,, \tag{S3}$$

Free active cofilin

$$\frac{dC}{dt} = J_C(t) - k_c C - f_{sev}(C, F_{old})\,, \tag{S4}$$

Cofilin severing rate

$$f_{sev}(C, F_{old}) = k_{sev} C_0 \left(\frac{C}{C_0}\right)^n \ell F_{old}\,, \tag{S5}$$

Free active Arp2/3

$$\frac{dA}{dt} = J_A(t) - k_a A - f_{nuc}(A, F_{new})\,, \tag{S6}$$

Arp2/3 binding rate

$$f_{nuc}(A, F_{new}) = k_{nuc} \frac{A}{K_m + A}\, \ell F_{new}\,. \tag{S7}$$

1.2 Additional Simulation Result

Simulation results shown in Fig. S1 are obtained by imposing a 10 s pulse of cofilin activation (step function $J_C(t)$), starting at $t = 2$ s. Cofilin level increases quickly and cofilin binds to old F-actin (F_{old}, initially at its low basal level). After a 5 s delay, the barbed end density increases and peaks at ∼13 s. This leads to the polymerization of new F-actin which achieves its maximum value at approximately 20 s. The new filaments then slowly age to F_{old}. Following stimulation, the system returns to its basal steady state (no active cofilin, no uncapped barbed ends, and low level of F-actin).

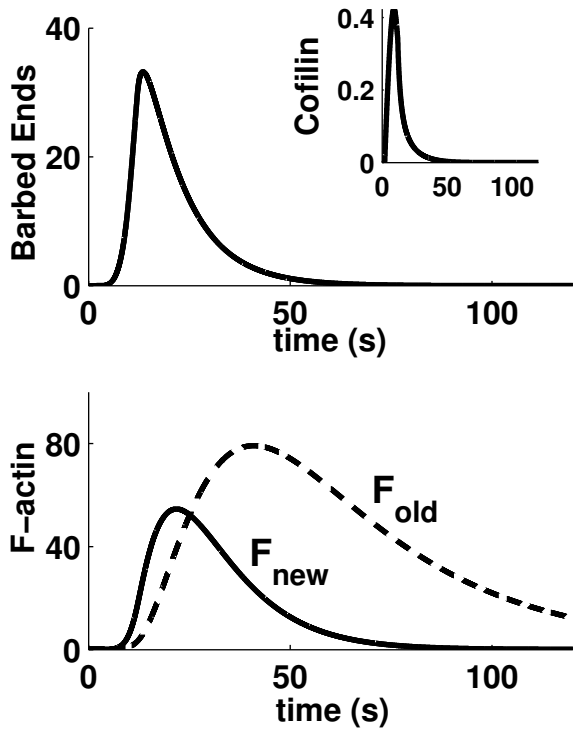

Figure S1: Dynamics of barbed ends, cofilin (inset) and F-actin following a high cofilin stimulus, obtained by a stimulus-induced flux of cofilin into the cell ($J_C = 0.1$ μM/s for $2 \leq t \leq 12$ s). Arp2/3 is absent here. Results are obtained using the basic parameter values listed in Table S1 and steady state initial conditions ($A(0) = 0$, $C(0) = 0$, $B(0) = 0$, $F_{new}(0) = J_f/k_{age}$, $F_{old} = J_f/k_{deg}$).

2 Full Spatial Model

Here we describe the full spatial model. For completeness, we provide the full equations, and details of boundary and initial conditions used. We also derive the coordinate transformation to a moving frame used in all simulations.

2.1 Equations

Length density of new F-actin (unit: $\mu\text{m}/\mu m^2$)

$$\frac{\partial F_{new}}{\partial t} = J_f - k_{age}\, F_{new} + V_0\, B\,, \qquad \text{[S8]}$$

Length density of old F-actin

$$\frac{\partial F_{old}}{\partial t} = k_{age}\, F_{new} - k_{deg}\, F_{old}\,, \qquad \text{[S9]}$$

Density of barbed ends (unit: $\#/\mu\text{m}^2$)

$$\frac{\partial B}{\partial t} = -\frac{\partial}{\partial x}\,(V_0 B) - k_{cap} B + \kappa(f_{sev} + f_{nuc})\,, \qquad \text{[S10]}$$

Concentration of free active Arp2/3 (unit: μM)

$$\frac{\partial A}{\partial t} = -\frac{\partial}{\partial x}\left(V_{mb}\, A\right) - f_{nuc}\left(C, F_{new}\right) - k_a A\,, \qquad \text{[S11]}$$

Concentration of free active cofilin (unit: μM)

$$\frac{\partial C}{\partial t} = D_c \frac{\partial^2 C}{\partial x^2} - \frac{\partial}{\partial x}\left(V_{mb}\, C\right) - f_{sev}\left(C, F_{old}\right) - k_c C\,. \qquad \text{[S12]}$$

Cofilin severing function f_{sev} and Arp2/3 binding rate f_{nuc} as in Eqns. [S5]-[S7].

Pushing barbed ends (unit: $\#/\mu$m)

$$\frac{dB_p}{dt} = (V_0 - V_{mb}) B(x_{edge}, t) - k_{cap} B_p\,, \qquad \text{[S13]}$$

Membrane protrusion rate (unit: μm/s)

$$V_{mb}(B_p) = V_0 \frac{B_p}{B_p + \phi \exp(\omega / B_p)}\,. \qquad \text{[S14]}$$

3 Implementation details for the spatial model

Our spatial model extends and improves that of Dawes et al. (1) for Arp2/3. First, we correct the boundary conditions for barbed ends and actin filaments at the cell edge, as discussed below. In the current formulation, conservation of barbed ends is maintained, and the number of actin filaments at the edge is consistent with the number of pushing barbed ends. Second, we correct the assumption that Arp2/3 can diffuse throughout the lamellipod. To reflect Arp2/3 activation occurring at the cell membrane, we use a Dirichlet boundary condition. We implemented the Arp2/3 PDE with a small "numerical" diffusion coefficient for Arp2/3 to avoid instabilities. This feature restricts Arp2/3 to within 0.1 μm of the cell edge. To reflect the release of active cofilin from its PIP_2 membrane-bound form (2), we used a finite flux boundary condition for cofilin. Details are described below.

3.1 Boundary and Initial Conditions

We impose the following boundary conditions:

- *Far field conditions*:
  For the barbed ends, we assume that inside the cell, far from the cell edge, the density of uncapped barbed ends is zero $B(-\infty, t) = 0$. We assume that there is no active Arp2/3 or cofilin far from the cell edge, $A(-\infty, t) = 0$ and $C(-\infty, t) = 0$. For all numerical simulations presented here, we take a domain of length 4 μm and impose these far field conditions at $x = x_{edge} - 4$ μm.

- *F-actin length density at x_{edge}*:
  The F-actin length density can be interpreted either as length of filaments per unit area (μm/μm^2) or as the number of filaments per μm across the width of the narrow transect ($\#/\mu$m). Right at the cell edge, the number of filaments per unit edge length must match the number of barbed ends per unit edge length, $B_p(t)$. We assume that

these pushing barbed ends are tips on new filaments, so $F_{new}\left(x_{edge}(t),t\right) = B_p(t)$ and $F_{old}\left(x_{edge}(t),t\right) = 0$. Note that these boundary conditions are needed following a coordinate transformation to a moving frame for the purpose of numerical simulation.

- *Activation for cofilin and Arp2/3 at the cell edge*:
  To simulate EGF stimulation, we use Neumann boundary conditions to reflect the release of active cofilin into the cell interior,

$$\left[-D_c\frac{\partial C}{\partial x} + V_{mb}\,C\right]_{x=x_{edge}} = \begin{cases} -J_C < 0 & \text{during stimulation } t \in [t_c, t_c + dt_c] \\ 0 & \text{otherwise,} \end{cases} \qquad \text{[S15]}$$

  Active Arp2/3 is bound to the WAVE2 complex on the cell membrane. We assume that activation simply increases the level of active Arp2/3 at the cell membrane:

$$A(x_{edge},t) = A_{edge}(t), = \begin{cases} A_{edge} > 0 & \text{during stimulation } t \in [t_a, t_a + dt_a] \\ 0 & \text{otherwise.} \end{cases} \qquad \text{[S16]}$$

Initial conditions are taken to be the unstimulated steady state values for cofilin, Arp2/3 and barbed ends:

$$C^{ss}(x) = 0,\ A^{ss}(x) = 0,\ B^{ss}(x) = 0,\ \text{and } V_{mb}^{ss} = 0,\ B_p^{ss} = 0, \qquad \text{[S17]}$$

The F-actin steady state distributions is $F_{new}^{ss} = J_f/k_{age}$ and $F_{old}^{ss} = J_f/k_{deg}$.

3.2 Derivation of Equation for B_p

We now derive the equation for the pushing barbed ends, B_p, based on a conservation principle. In the absence of creation or capping of barbed ends, the *total* number of barbed ends should be conserved. The total number of barbed ends across the lamelipod, including pushing barbed ends is given by

$$B_{total} = \int_{-\infty}^{x_{edge}(t)} B(x,t)dx + B_p(t).$$

To obtain conservation, we must enforce

$$\frac{d}{dt}B_{total} = 0, \quad \Rightarrow \quad \frac{d}{dt}\int_{-\infty}^{x_{edge}(t)} B(x,t)dx = -\frac{d}{dt}B_p(t).$$

Using [S10] and integrating over space, note that

$$\begin{aligned} \frac{d}{dt}\left[\int_{-\infty}^{x_{edge}(t)} B(x,t)dx\right] &= \int_{-\infty}^{x_{edge}(t)} \frac{\partial B}{\partial t}dx \;+\; B(x_{edge}(t),t)\,\frac{dx_{edge}}{dt} \\ &= \int_{-\infty}^{x_{edge}(t)} -V_0\frac{\partial B}{\partial x}dx + V_{mb}\cdot B(x_{edge}(t),t) \\ &= -V_0\Big[B(x_{edge}(t),t) - B(-\infty,t)\Big] + V_{mb}\cdot B(x_{edge}(t),t) \\ &= (V_{mb} - V_0)\,B(x_{edge}(t),t). \end{aligned}$$

Thus for conservation, we arrive at an ODE for the pushing barbed ends, $B_p(t)$,

$$\frac{dB_p}{dt} = (V_0 - V_{mb})B(x_{edge}(t), t). \quad \text{[S18]}$$

Allowing for capping, we obtain Eqn. [S13], and this is used to close the system.

3.3 Arp2/3: Numerical Diffusion

In order to impose the boundary conditions associated with stimulation at the cell edge, we modified the hyperbolic Arp2/3 equation [S11] with numerical diffusion (a common practice in treating such PDEs numerically),

$$\frac{\partial A}{\partial t} = \epsilon \frac{\partial^2 A}{\partial x^2} - \frac{\partial}{\partial x}\left(V_{mb}\, A\right) - f_{nuc}\left(C, F_{new}\right) - k_a A.$$

We chose the value of the small parameter $\epsilon = 0.0001\ \mu\text{m}^2/\text{s}$ such that Arp2/3 is restricted to within a thin region $< 0.1\ \mu$m of the cell edge. This thickness is likely an overestimate. However, it makes computations on a reasonable grid feasible. Later on we discuss how decreasing the region of Arp2/3 influence affects our conclusions.

3.4 Transforming to Moving Coordinate System

For numerical simulations, we change the coordinate system from a static "lab" frame (x, t) to a frame moving with the cell edge, $(z(t), t)$ where $z(t) = x - x_{edge}(t)$ is a position relative to the cell edge. Then, for any function $G(z(t), t)$, the rate of change is given by the material derivative,

$$\frac{DG}{Dt} = \frac{\partial G}{\partial t} + \frac{\partial G}{\partial z}\cdot\frac{dz}{dt} = \frac{\partial G}{\partial t} - \frac{\partial G}{\partial z}\cdot\frac{dx_{edge}}{dt} = \frac{\partial G}{\partial t} - V_{mb}(t)\frac{\partial G}{\partial z}. \quad \text{[S19]}$$

Note that here, V_{mb} is not constant nor prescribed a priori, and that it depends on the number of pushing barbed ends (Eqs. [S13]-[S14]), itself a dynamic variable. Following this formal change of coordinate, the cell edge corresponds to $z = 0$. The full system now can be written as,

$$\begin{aligned}
\frac{\partial B}{\partial t} &= -\frac{\partial}{\partial z}\Big[(V_0 - V_{mb})B\Big] - k_{cap}\, B + \kappa(f_{sev} + f_{nuc}), && \text{[S20]}\\
\frac{\partial F_{new}}{\partial t} &= V_{mb}\,\frac{\partial F_{new}}{\partial z} + V_0\, B - k_{age}\, F_{new}, && \text{[S21]}\\
\frac{\partial F_{old}}{\partial t} &= V_{mb}\,\frac{\partial F_{old}}{\partial z} + k_{age}\, F_{new} - k_{deg}\, F_{old}, && \text{[S22]}\\
\frac{\partial C}{\partial t} &= D_c\frac{\partial^2 C}{\partial z^2} - f_{sev}\left(C, F_{old}\right), && \text{[S23]}\\
\frac{\partial A}{\partial t} &= \epsilon\frac{\partial^2 A}{\partial z^2} - f_{nuc}\left(C, F_{old}\right), && \text{[S24]}
\end{aligned}$$

where variables are now functions of both $z(t)$ and t. It is interesting to note that this set of equations describes an "apparent" drift of F-actin rearwards (as it is left behind when the

cell edge moves forward), a motion of barbed ends towards the cell edge (with relative speed $(V_0 - V_{mb})$) and simple diffusion of cofilin. The numerical Arp2/3 diffusion is also preserved.

Numerical approximation of the solution of this system is obtained by discretizing using a finite difference scheme. Diffusion terms are discretized using a Crank-Nicolson method and advection terms are discretized using an explicit first-order upwind scheme. Reaction terms are implemented explicitly in the discretized system. Our computational domain reflects the first 4 μm from the cell edge. We chose a spatial step size of $\delta x = 4/2000 = 0.002$ μm, and a time-step of $\delta t \leq 0.001$ s is chosen for stability.

4 Parameter Estimation

In Table S1, we list the parameter values and their sources. The values are inferred from existing literature as discussed below.

4.1 Actin Dynamics Parameters

We assume that over the timescale of the stimulation, monomer availability is not limiting, so that polymerization velocity is roughly constant. We take $V_0 \approx 0.3$ μm/s, a typical value as estimated in (3, 4).

We make a simplifying assumption that capping of barbed ends occurs at an equal rate everywhere. In (3), it was estimated that at a typical cellular concentration of capping protein, a free barbed end has a half life of ~ 0.25 s before being capped (maximum capping rate of $\ln(2)/0.25$ s ≈ 2.77/s). However, barbed-end capping near the membrane is reduced to $\sim$0.1/s. Here we assume $k_{cap} = 1$/s as in (1).

Full ATP to ADP actin conversion takes 10-30 s (3), and we take $k_{age} = 0.1$/s. The half life of actin filaments within the lamellipodia of fibroblasts, fish keratocytes and nerve growth cones is estimated to be 0.5-3 min ((3, 11)), we take $k_{deg} = \ln(2)/23$ s ≈ 0.03/s (1, 5). This parameter reflects a combined turnover rate of F-actin and includes various cofilin-independent processes such as depolymerization, debranching, and fragmentation.

The parameters ω and ϕ describing the dependence of the protrusion rate V_{mb} on the number of pushing barbed ends, were taken directly from (6) (see equation (24) in their Supplementary Material for derivation and discussion).

In this model, we assume that there is no cofilin and Arp2/3 activity when the cell is at rest (basal unstimulated state). Thus, we assume a very low density of F-actin at rest, attributed to de-novo nucleation by other sources such as formin (12), taking $J_f = 0.01/\mu$m s.

4.2 Scale Factors

We consider a 1 μm-wide transect of a lamellipod that has constant thickness 0.18 μm, and length 10 μm (13). The units for cytoskeletal variables (F-actin and barbed ends) are number or length per unit area averaged over the thickness of the transect. The constant κ represents a scale factor for change of units between concentration, in μM, and barbed end density, B, in $\#/\mu\text{m}^2$. A concentration of 1 μM corresponds to 602 molecules/μm^3.

Table S1: List of parameter values and their sources. E_0: primary experimental literature, M: pre-existing models, E_2: values used in previous models but based on experimental literature.

Parameters	Definitions	Values	Source
V_0	free polymerization speed	0.3 μm/s	E_0: (3, 4)
k_{cap}	capping rate	1 /s	M, E_2: (1)
k_{age}	rate of filament aging	0.1 /s	E_0: (3)
k_{deg}	bulk filament turnover rate	0.03 /s	E_0, M: (1, 3, 5)
ω	physical parameter describing membrane resistance	50 /μm	E_0: (6)
ϕ	geometric parameter used in computing protrusion rate	10 /μm	E_0, M: (6)
J_f	basal actin nucleation rate	0.01 /μm.s	M: small value
D_c	diffusion coefficient of cofilin	10 μm^2/s	E_0, M: (5, 7)
ϵ	numerical diffusion coefficient of Arp2/3	0.0001 μm^2/s	this paper
κ	scale factor converting concentrations to units of B	106 /μm$^2 \cdot \mu$M	M: (5)
ℓ	scale factor converting units of F to concentration	0.255 μM·μm	M: (5)
k_{nuc}	Arp2/3 nucleation rate	60/ℓ /s	E_2, M: (5)
K_m	saturation constant for Arp2/3 nucleation	2 μM	M: (5)
k_{sev}	severing rate for cofilin	0.01/μM·s	E_0: (8, 9)
C_0	threshold for cofilin cooperative severing	0.1 μM	E_0: (8, 9)
n	degree of cofilin cooperative severing	4	M: (10)
k_a	basal Arp2/3 degradation rate	0.1/s	M: (5)
k_c	basal cofilin degradation rate	0.1/s	M: (10)
J_c	Inward active cofilin edge flux	0-10 μM·μm/s	values varied
A_{edge}	Active Arp2/3 edge concentration	0-10 mM	values varied

Assuming a lamellipodium of thickness 0.18 μm, a concentration of 1 μM gives $\kappa = 0.18\ \mu\text{m} \cdot (602\ \text{molecules}/\mu\text{m}^3)/(1\mu\text{M}) \approx 106\ \text{molecules}\ /\mu\text{m}^2 \cdot \mu\text{M}$.

The scale factor ℓ is used to convert units of F-actin (length per unit area, $\mu\text{m}/\mu\text{m}^2 = \mu\text{m}^{-1}$) to that of Arp2/3 concentration (5). As derived for κ, we take 1 μM of actin to correspond to 106 monomers/μm^2 lamellipodial area. Now, one monomer contributes to 0.027 μm of filament length. Thus, 1 μm of filament length per 1 μm^2 area corresponds to $1/(0.027 \times 106) = 0.349$ μM of monomers. A minimal distance of approximately 37 nm (23.7 monomers) has been observed between side branches along a single filament (14, 15), so 1μM Arp2/3 approximately binds to 13.7 μM of F (expressed in terms of monomers). Thus, the scale factor for the conversion between F-actin length density to Arp2/3 concentration is $\ell = 0.349/13.7 = 0.255$ μM μm.

Although, the scale factor ℓ just derived takes into account the minimal distance between branches nucleated by Arp2/3 along a filament, for simplicity, we use the same conversion factor ℓ to scale between F-actin and cofilin concentration. The minimal distance between cofilin binding sites along an actin filament can vary. A recent model proposed that multiple cofilin molecules bind cooperatively along an F-actin filament (8, 16). The binding of the first cofilin molecule is slow and dependent upon the fluctuations along the filament, but this then allows rapid subsequent cofilin binding. Boundaries are created between "cofilin-decorated" sections which then promotes severing (8, 16). We do not take into account the physical details of cofilin binding and severing.

4.3 Cofilin and Arp2/3 Parameters

The diffusion coefficient of G-actin (molecular weight of 40 kDa) in the cytosol has been estimated to be 5 μm^2/s (5, 17). Here we take the diffusion coefficient of the smaller protein, cofilin (21 kDa (7)) to be 10 μm^2/s.

The cofilin severing function f_{sev} is discussed in (10), but here parameter values are based on previous in vitro studies (9) and a recent stochastic model of actin length regulation in the presence of cofilin (8). In our model, we take C_0, the threshold for cofilin cooperative severing to be 0.1 μM, based on the dissociation constant for amoeba cofilin bindin to ADP-actin in vivo (9). This value also falls between the dissociation constant of the first cofilin binding ($K_d = 0.59$ μM) and the dissociation constant for the cooperative binding ($K_d^{coop} = 0.067$ μM) given in the detailed stochastic binding model (8). We take a characteristic actin monomer concentration where filaments grow (rather than depolymerize) to be 1 μM, and take the severing rate to be $k_{sev} = 0.01$/s (per μM actin) as in (8).

We assume the same Arp2/3 binding kinetics as in (5). The Arp2/3 nucleation function f_{nuc} is based on a quasi steady state approximation of the following reaction scheme

$$A + \ell F_{new} \underset{k_-}{\overset{k_+}{\rightleftharpoons}} C \xrightarrow{k_2} \ell F_{new} + \kappa B\,, \qquad \text{[S25]}$$

with the assumption that Arp2/3 is a limiting factor (then $K_m = k_-/k_+$ and $k_{nuc} = k_2$). We take a small Arp2/3 inactivation rate, $k_a = 0.1$/s as in (5) and a similar value for for cofilin ($k_c = 0.1$/s); this value is within the range obtained from data-fitting in (10).

5 Spatial Distribution of Barbed End Production

Spatial distribution of severing (f_{sev}) and nucleation (f_{nuc}) rates over time are shown in Fig. S2. The spatial extent of cofilin ($\sim 1\ \mu$m) is an order of magnitude larger than that of Arp2/3 in our model, though both peak at the cell edge.

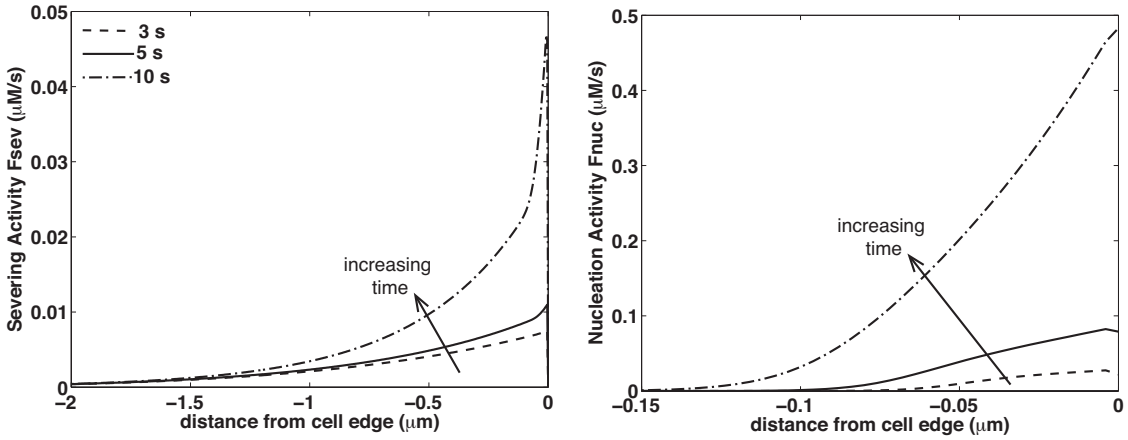

Figure S2: Spatially distributed production of barbed ends: severing by cofilin $f_{sev}(x,t)$ (left), and branching by Arp2/3, $f_{nuc}(x,t)$ (right), at several time points during simulation. Parameters, boundary and initial conditions as in Fig. 3.

6 Effect of Tropomyosin

We considered the effect of tropomyosin which has been shown to compete with cofilin for binding sites along old ADP-F-actin and then protect the filament from severing by cofilin (18). DesMarais et al. (19) showed that level increases from the cell front to the interior (4.5 μm inside) with very little tropomyosin found near the very cell edge.

We incorporated these effects into our mathematical model using the simplest possible assumption to avoid significantly expanding the model. We assume that tropomyosin binding removes available cofilin binding sites on old F-actin, so now

$$\frac{\partial F_{old}}{\partial t} = k_{age}\, F_{new} - (k_{deg} + d_T(x))F_{old}\,, \qquad \text{[S26]}$$

where $d_T(x)$ represents a spatial distribution of tropomyosin which we take to be a linear function (as shown in the top panel of Fig. S3A) similar to the data in (19). We also tracked a third class of F-actin, namely the tropomyosin-protected filaments, F_{tm}.

$$\frac{\partial F_{tm}}{\partial t} = d_T(x)F_{old}\,. \qquad \text{[S27]}$$

In constructing $d_T(x)$, we have chosen a binding rate $T = 5/\text{s}$ away from the cell edge (at 4 μM inside). Wegner and Ruhnau (20) found that at 10 μM tropomyosin concentration, the association rate constant were 2.5-4/μM·s.

The effect of tropomyosin in localizing and limiting the cofilin response are shown in simulation results of Fig. S3. In the bottom panel of Fig. S3A, we plotted the severing rate f_{sev} across the lamellipodial transect at 10 s after stimulation. We found that in the presence of tropomyosin, cofilin activity is reduced, resulting in lower f_{sev} values and that severing activity is more localized towards the front of the cell. While peak severing activity is found at the cell edge with or without tropomyosin, the cofilin activity is contained to within 0.5 μm from the edge in the presence of tropomyosin.

In Fig. S3B, we show the barbed end production curves for cofilin or Arp2/3 acting alone, in the presence/absence of tropomyosin. In this model variant, tropomyosin only affects cofilin activity and its effect on Arp2/3 (21) has not been included. Barbed end production by cofilin is reduced in the presence of tropomyosin. However, the shape of the barbed end production curve with wide sensitive region is retained and thus high synergy and large barbed end production can still be obtained.

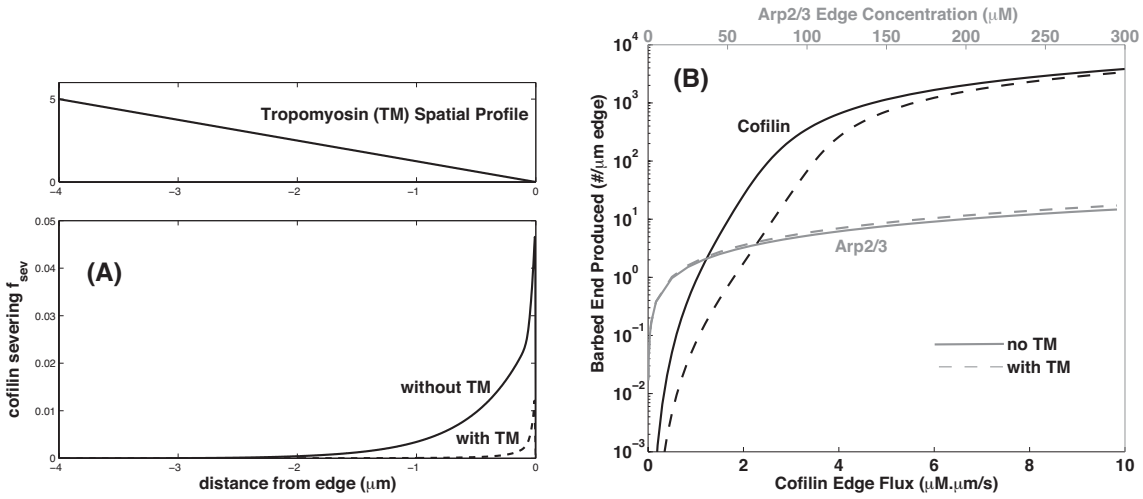

Figure S3: Effects of tropomyosin. **(A)** Top: Assumed spatial profile of tropomyosin in the revised model. Bottom: Rate of barbed end creation by cofilin severing of actin, f_{sev}, across the lamellipod at 10 s after stimulation (with and without tropomyosin). **(B)** The effect of cofilin (Arp2/3) activation release flux at the membrane on barbed end production by cofilin (Arp2/3) acting alone. A qualitatively similar barbed end production is obtained despite tropomyosin inhibition of cofilin. (Compare to Fig. 4A in main paper.)

7 Parameter Sensitivity Tests

Here we report the effects of varying several key parameters, including the F-actin aging rate k_{age}, the barbed end capping rate k_{cap}, and the free polymerization rate V_0.

7.1 Effect of Filament Aging Rate k_{age}

Although the ATP nucleotide is not essential for polymerization of monomers into F-actin (22), its hydrolysis and phosphate dissociation is a "timer" for filament age (4). Once an ATP-G-actin monomer is assembled onto an F-actin polymer, ATP hydrolysis to ADP-Pi is fast (1-3 s (23)). Phosphate (Pi) release, resulting in ADP-F-actin, occurs more slowly (minutes in vitro (24, 25)). Recent studies using microfluidics in the presence of profilin, suggest that Pi release occurs stochastically with a half-life of 102 s (26). However, it has been suggested that Pi release occurs 10 times faster in vivo (3). Cofilin appears to accelerate the release of the phosphate group (9, 27).

We tested the effect of the filament aging timescale. Here we assume that cofilin binds only to ADP-F-actin and Arp2/3 to ATP-F-Actin. In Fig. S4 we show how varying k_{age} in [S8]-[S9] affects barbed end production and synergy. On the left panel, we show barbed end production B_{prod} in the presence of either cofilin or Arp2/3 alone. As k_{age} increases, cofilin severing activity increases because the level of old F-actin increases (making more substrate available for cofilin binding and severing). On the other hand, as k_{age} increases, barbed end production due to Arp2/3 nucleating decreases. On the right panel of Fig. S4, we show barbed end production and synergy in the presence of both cofilin and Arp2/3. Barbed end production increases monotonically with k_{age} and the contribution from cofilin dominates for large k_{age}. However, maximum synergy occurs when $k_{age} \approx 0.12$/s which, interestingly, coincides with the k_{age} rate observed in vivo.

7.2 Effect of Barbed End Capping Rate k_{cap}

Increasing the capping rate, k_{cap}, reduces barbed end production (Fig. S5). We first considered the case when cofilin or Arp2/3 act alone. In that case, we find that barbed end production by Arp2/3 decreases as k_{cap} is increased. Faster capping leads to an overall reduction in the level of new filaments. However barbed end production is not affected significantly when cofilin or Arp2/3 act alone. Doubling the capping rate k_{cap} from 0.1/s to 0.2/s leads only to a 2% (3%) decrease in barbed end production for Arp2/3 (cofilin). However, when cofilin and Arp2/3 work together, capping affects barbed end production significantly. Doubling the capping rate k_{cap} from 0.1/s to 0.2/s leads to a 30% decrease in total barbed end production. This in turn affects cell protrusion as indicated by a sharp decrease in the maximal protrusion rate (a decrease from 0.07 μm/2 to 0.002 μm/s). Synergy also decreases monotonically as k_{cap} is increased (S drops from 4.8 to 3.8 when k_{cap} is doubled from 0.1/s to 0.2/s).

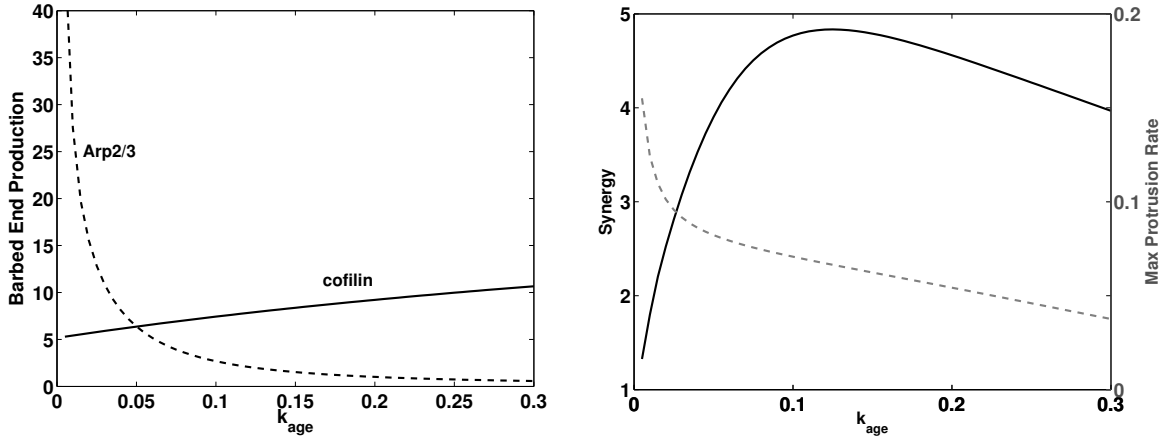

Figure S4: Effect of the F-actin aging rate k_{age} on barbed end production and synergy. Left: Barbed end production (B_{prod}) in the presence of cofilin only (solid curve) and Arp2/3 only (dashed curve). Right: Synergy (black solid curve, left axis) and barbed end production (grey dashed curve, right axis) in the presence of both cofilin and Arp2/3. ($J_C = 1.6$ μM·μm/s, $A_{edge} = 44$ μM, as in Fig. 3), simultaneous cofilin and Arp2/3 stimulation ($0 < t < 10$s). Other parameters as in Table S1.

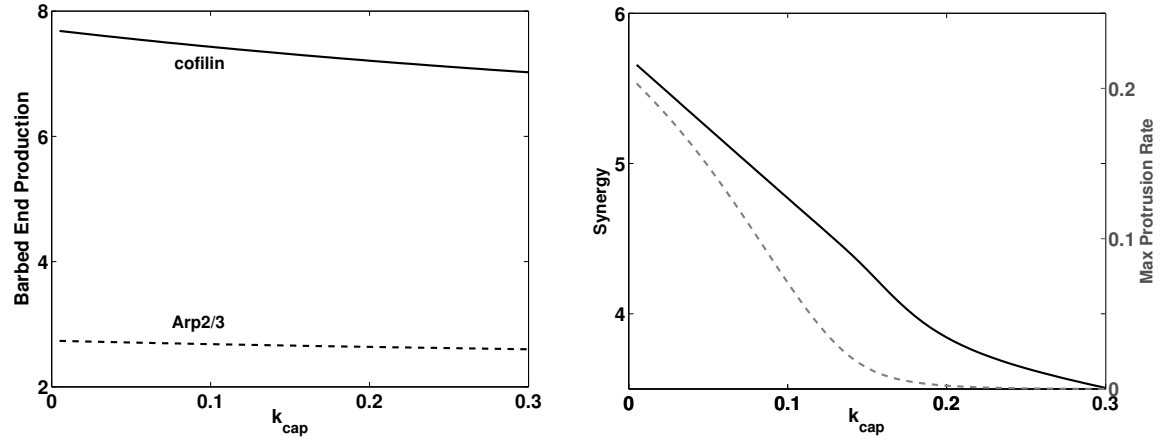

Figure S5: Effect of barbed end capping rate k_{cap} on barbed end production and synergy. Left: Barbed end production (B_{prod}) in the presence of cofilin alone (grey dashed curve, right axis) and Arp2/3 alone (black solid curve, left axis). Right: Synergy (black solid curve, left axis) and barbed end production (grey dashed curve, right axis) in the presence of both cofilin and Arp2/3. ($J_C = 1.6$ μM·μm/s, $A_{edge} = 44$ μM, as in Fig. 3), simultaneous cofilin and Arp2/3 stimulation ($0 < t < 10$s). Other parameters as in Table S1.

7.3 Capping, Aging and Polymerization Speed

We vary capping, filament aging and polymerization speed over a wide range of biologically relevant values, and show the resultant synergy and barbed end production in Fig. S6. Varying k_{cap} and k_{age} (top panels), we find higher barbed end production when k_{cap} is low (slow capping), consistent with previous results of Fig. S5. However, at a given capping rate, high synergy is only found when the filament aging rate, k_{age} is low (slow aging). For the given stimulation size, barbed end production is dominated by Arp2/3. Cofilin simply primes the system by generating new F-actin. We varied the polymerization speed V_0 and capping rate k_{cap} (middle panels). Increasing the polymerization speed increases both synergy and barbed end production. As before, slower capping promotes actin growth. A similar trend is observed when we vary both polymerization speed and filament aging rate (bottom panels).

To summarize, slower caping and filament aging increase both barbed end production and the level of synergy between cofilin and Arp2/3. Faster polymerization speed increases actin growth as well. However, polymerization speed is limited by availability of G-actin monomer, a factor that is not currently represented in our model.

7.4 Arp2/3 Localization parameter (ϵ)

As previously discussed, numerical diffusion (parameter ϵ) in the Arp2/3 equation is used to avoid discontinuities and singularities from developing in the numerical solution. Using a very small value of ϵ then mandates a very fine spatial grid, which increases computation time prohibitively. For this reason, we carried out only limited tests with a reduced value of $\epsilon = 10^{-6}$ μm/s, where Arp2/3 is highly localized to well within 0.01 μm of the cell edge as shown in Movie S3. Barbed end production and synergy results are shown in Fig. S7. From the barbed end production curve, we observe that a much higher Arp2/3 edge-concentration is required to generate a given number barbed ends. Additionally, narrow localization of Arp2/3 limits barbed end production that can be attained; the maximal (plateau) barbed end production level obtained is approximately one order of magnitude lower in comparison to that obtained using ($\epsilon = 10^{-4}$). When Arp2/3 and cofilin are both present, synergy occurs allowing Arp2/3 to generate more barbed ends. From our numerical simulation, the maximal level of synergy observed is ~ 2.6 ($A_{edge} = 2000$ and $J_c = 4$) but this stimulation amplitude leads to low maximum protrusion rate (0.01μm/s). High barbed end production and high synergy can be obtained still by increasing the cofilin edge flux slightly, as shown in the right panel of Fig. S7 ($V_{max} = 0.11$ μm/s here).

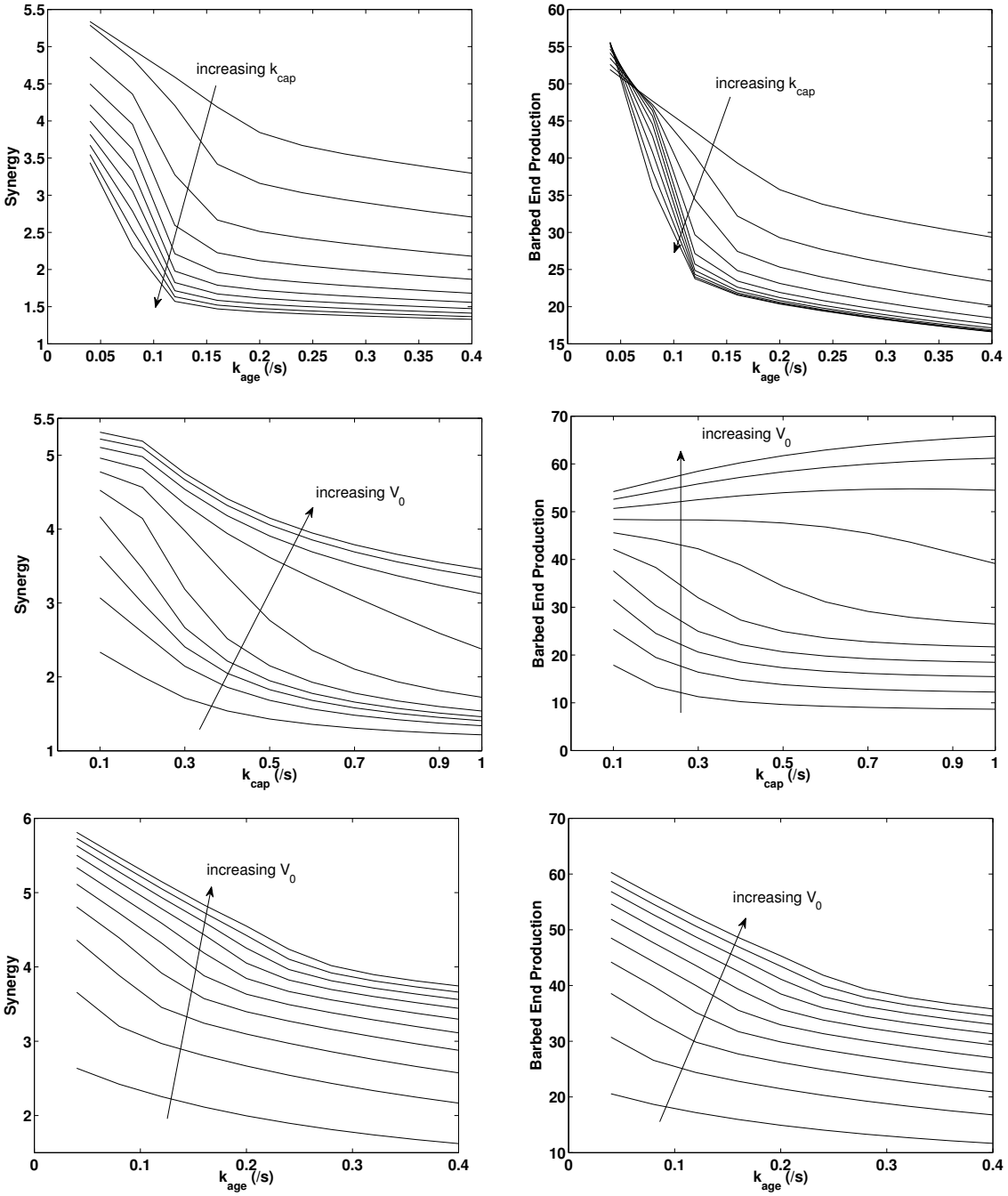

Figure S6: Effects of caping rate k_{cap}, filament aging rate k_{age}, and polymerization speed V_0 on synergy (left panels) and total barbed end production (right panels) ($J_C = 1.6$ μM·μm/s, $A_{edge} = 44$ μM, simultaneous cofilin and Arp2/3 activation for 10 s, but k_{cap}, k_{age} and V_0 varied. Other parameters as in Table S1).

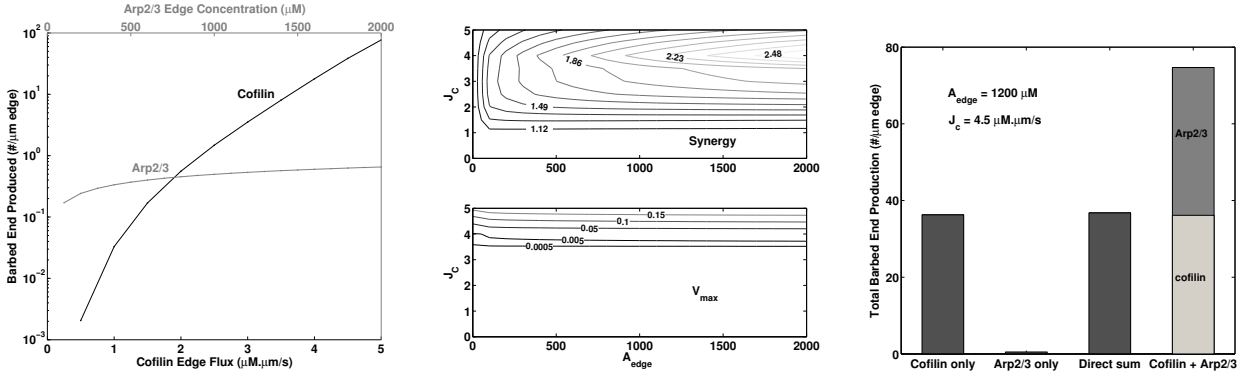

Figure S7: Barbed end production and synergy with highly localized Arp2/3 ($\epsilon = 10^{-6}$ μm/s). Left: Barbed end production curve when cofilin and Arp2/3 act alone. Middle: Synergy and maximum protrusion rate for varying stimulation amplitude. Right: Comparison of total barbed end production using stimulation size of $A_{edge} = 1200$ and $J_c = 4.5$ (S=2.03).

8 Effect of Cofilin Binding to New Filaments

Previous work found that cofilin binds slowly to new F-actin, accelerates release of the phosphate group on ADP-Pi actin filaments (27) and thereby promotes debranching and Arp2/3 dissociation from older filaments (27, 28). Here we explored only the effect of cofilin severing new filaments, rather than its influence on filament aging. This extension can be explored in the future.

Our approach parallels the treatment of Arp2/3 binding, as in Eqn. [19] in the main manuscript. We modified the cofilin severing term to

$$f_{sev}(C, F_{new}, F_{old}) = (1-\beta)k_{sev}C_0\left(\frac{C}{C_0}\right)^n \ell F_{old} + \beta k_{sev}C_0\left(\frac{C}{C_0}\right)^n \ell F_{new}\,. \qquad \text{[S28]}$$

where $0 \leq \beta \leq 1$ reflects preferential binding of cofilin to new versus old F-actin. When $\beta = 0$, cofilin only binds to F_{old} as in our previous basic model. When $\beta > 0$, cofilin can also sever new filaments.

Dependence on β is illustrated in Fig. S8. Neither synergy nor barbed end production is affected significantly as β is varied. As β increases, barbed end production (as reflected by the protrusion rate) slightly increases up to $\beta \approx 0.6$ then slightly decreases thereafter. A higher level of new F-actin is found at the cell edge where cofilin is also activated; thus cofilin can sever more filaments and generate more barbed ends. At high value of β, barbed end production decreases because the older filaments are no longer effective substrate for cofilin severing activity.

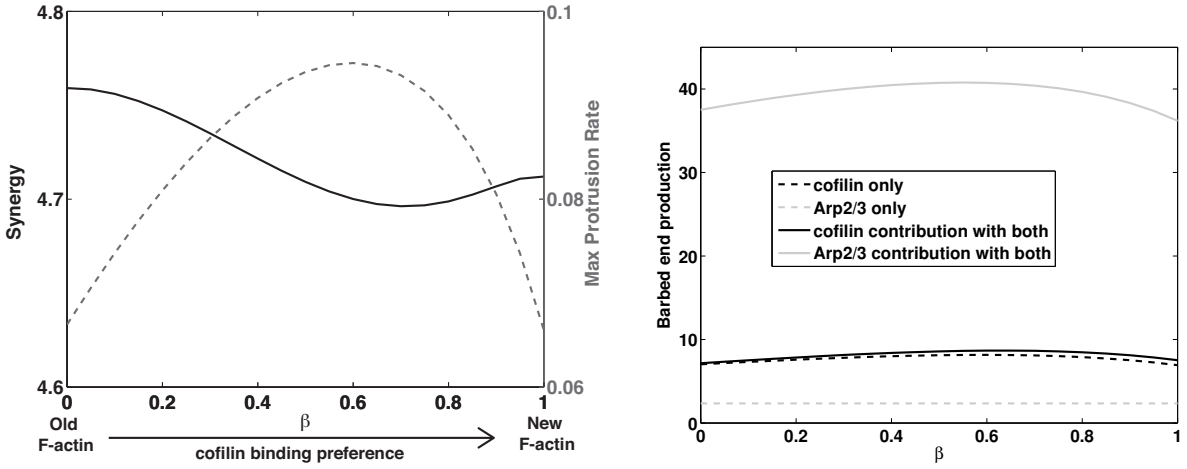

Figure S8: Effect of Cofilin binding to new (ATP) versus old (ADP) F-actin, depicted by β in Eqn. [S28]. Left: Maximum protrusion rate V_{max} (in dashed grey, right axis) and synergy (in solid black, left axis) versus β. Right: Comparison of barbed end production by cofilin ($\int\int f_{sev}\, dxdt$) and by Arp2/3 ($\int\int \overline{f_{nuc}}\, dxdt$) as β is varied. ($J_C = 1.6$ μM·μm/s, $A_{edge} = 44$ μM, simultaneous cofilin and Arp2/3 activation for 10 s, but with Arp2/3 barbed end production rate defined in Eqn. [S28]. Other parameters as in Table S1).

9 List of Movies

- **Movie 1** - Spatio-temporal dynamics of variables following simultaneous cofilin and Arp2/3 stimulation. This movie is analogous to Fig. 3. Top panel: F_{new} is solid line and F_{old} in dashed line.

- **Movie 2** - Spatio-temporal dynamics of variables following a cofilin activation and a delayed Arp2/3 stimulation (t_{arp}=11.5 s). Parameter values as in Fig. 5 B. Top panel: F_{new} is solid line and F_{old} in dashed line.

- **Movie 3** - Spatio-temporal dynamics of variables following simultaneous cofilin and Arp2/3 stimulation obtained using $\epsilon = 10^{-6}$ leading to narrow Arp2/3 localization near the cell edge. This movie corresponds to the right panel of Fig. S7 ($A_{edge} = 1200\mu$m and $J_C = 4.5\mu$M.μm/s. All other parameter values are as listed in Table S1). Top panel: F_{new} is solid line and F_{old} in dashed line.

References

1. Dawes, A. T., G. Bard Ermentrout, E. N. Cytrynbaum, and L. Edelstein-Keshet, 2006. Actin filament branching and protrusion velocity in a simple 1D model of a motile cell. *J Theor Biol.* 242:265–79.

2. van Rheenen, J., X. Song, W. van Roosmalen, M. Cammer, X. Chen, V. Desmarais, S.-C. Yip, J. M. Backer, R. J. Eddy, and J. S. Condeelis, 2007. EGF-induced PIP2 hydrolysis releases and activates cofilin locally in carcinoma cells. *J Cell Biol.* 179:1247–59.

3. Pollard, T. D., L. Blanchoin, and R. D. Mullins, 2000. Molecular mechanisms controlling actin filament dynamics in nonmuscle cells. *Annu Rev Biophys Biomol Struct.* 29:545–76.

4. Pollard, T., and G. Borisy, 2003. Cellular motility driven by assembly and disassembly of actin filaments. *Cell.* 112:453–465.

5. Marée, A., A. Jilkine, A. Dawes, V. Grieneisen, and L. Edelstein-Keshet, 2006. Polarization and movement of keratocytes: a multiscale modelling approach. *Bull Math Biol.* 68:1169–1211.

6. Lacayo, C. I., Z. Pincus, M. M. VanDuijn, C. A. Wilson, D. A. Fletcher, F. B. Gertler, A. Mogilner, and J. A. Theriot, 2007. Emergence of large-scale cell morphology and movement from local actin filament growth dynamics. *PLoS Biol.* 5:e233.

7. Nishida, E., S. Maekawa, and H. Sakai, 1984. Cofilin, a protein in porcine brain that binds to actin filaments and inhibits their interactions with myosin and tropomyosin. *Biochemistry-US.* 23:5307–5313.

8. Roland, J., J. Berro, A. Michelot, L. Blanchoin, and J.-L. Martiel, 2008. Stochastic Severing of Actin Filaments by Actin Depolymerizing Factor/Cofilin Controls the Emergence of a Steady Dynamical Regime. *Biophys J.* 94:2082 – 2094.

9. Blanchoin, L., and T. D. Pollard, 1999. Mechanism of Interaction of Acanthamoeba Actophorin (ADF/Cofilin) with Actin Filaments. *J Biol Chem.* 274:15538–15546.

10. Tania, N., E. Prosk, J. Condeelis, and L. Edelstein-Keshet, 2011. A temporal model of cofilin regulation and the early peak of actin barbed ends in invasive tumor cells. *Biophys J.* 100:1883 – 1892.

11. Welch, M. D., and R. D. Mullins, 2002. Cellular Control of Actin Nucleation. *Annu Rev Cell Dev Bio.* 18:247–288.

12. Zigmond, S. H., 2004. Formin-induced nucleation of actin filaments. *Curr Opin Cell Biol.* 16:99 – 105.

13. Abraham, V. C., V. Krishnamurthi, D. L. Taylor, and F. Lanni, 1999. The Actin-Based Nanomachine at the Leading Edge of Migrating Cells. *Biophys J.* 77:1721 – 1732.

14. Mullins, R. D., J. A. Heuser, and T. D. Pollard, 1998. The interaction of Arp2/3 complex with actin: Nucleation, high affinity pointed end capping, and formation of branching networks of filaments. *Proc Natl Acad Sci USA.* 95:6181–6186.

15. Svitkina, T., and G. Borisy, 1999. Arp2/3 complex and actin depolymerizing factor/cofilin in dendritic organization and treadmilling of actin filament array in lamellipodia. *J Cell Biol.* 145:1009.

16. De La Cruz, E., and D. Sept, 2010. The kinetics of cooperative cofilin binding reveals two states of the cofilin-actin filament. *Biophys J.* 98:1893 – 1901.

17. Novak, I., B. Slepchenko, and A. Mogilner, 2008. Quantitative analysis of g-actin transport in motile cells. *Biophys J.* 95:1627–1638.

18. Ono, S., and K. Ono, 2002. Tropomyosin inhibits ADF/cofilin-dependent actin filament dynamics. *J Cell Biol.* 156:1065–1076.

19. DesMarais, V., I. Ichetovkin, J. Condeelis, and S. E. Hitchcock-DeGregori, 2002. Spatial regulation of actin dynamics: a tropomyosin-free, actin-rich compartment at the leading edge. *J Cell Sci.* 115:4649–4660.

20. Wegner, A., and K. Ruhnau, 1988. Rate of binding of tropomyosin to actin filaments. *Biochemistry-US.* 27:6994–7000.

21. Blanchoin, L., T. D. Pollard, and S. E. Hitchcock-DeGregori, 2001. Inhibition of the Arp2/3 complex-nucleated actin polymerization and branch formation by tropomyosin. *Curr Biol.* 11:1300 – 1304.

22. De La Cruz, E., A. Mandinova, M. Steinmetz, D. Stoffler, U. Aebi, and T. Pollard, 2000. Polymerization and structure of nucleotide-free actin filaments. *J Mol Biol.* 295:517–526.

23. Blanchoin, L., and T. Pollard, 2002. Hydrolysis of ATP by polymerized actin depends on the bound divalent cation but not profilin. *Biochemistry-US.* 41:597–602.

24. Carlier, M., and D. Pantaloni, 1986. Direct evidence for ADP-Pi-F-actin as the major intermediate in ATP-actin polymerization. Rate of dissociation of Pi from actin filaments. *Biochemistry-US.* 25:7789.

25. Melki, R., S. Fievez, and M.-F. Carlier, 1996. Continuous monitoring of pi release following nucleotide hydrolysis in actin or tubulin assembly using 2-amino-6-mercapto-7-methylpurine ribonucleoside and purine-nucleoside phosphorylase as an enzyme-linked assay. *Biochemistry-US.* 35:12038–12045.

26. Jégou, A., T. Niedermayer, J. Orbán, D. Didry, R. Lipowsky, M. Carlier, and G. Romet-Lemonne, 2011. Individual actin filaments in a microfluidic flow reveal the mechanism of ATP hydrolysis and give insight into the properties of profilin. *PLOS Biol.* 9:e1001161.

27. Blanchoin, L., T. Pollard, and R. Mullins, 2000. Interactions of ADF/cofilin, Arp2/3 complex, capping protein and profilin in remodeling of branched actin filament networks. *Curr Biol.* 10:1273–1282.

28. Chan, C., C. C. Beltzner, and T. D. Pollard, 2009. Cofilin Dissociates Arp2/3 Complex and Branches from Actin Filaments. *Curr Biol.* 19:537 – 545.